2006

Comparative study of axial flux permanent magnet brushless DC motor operating with the winding connected in single-phase and two-phase system

Sunil Kumar Challa
Louisiana State University and Agricultural and Mechanical College, schall2@lsu.edu

COMPARATIVE STUDY OF AXIAL FLUX PERMANENT MAGNET BRUSHLESS DC MOTOR OPERATING WITH THE WINDING CONNECTED IN SINGLE-PHASE AND TWO-PHASE SYSTEM

A Thesis
Submitted to the Graduate Faculty of the
Louisiana State University
And Agricultural and Mechanical college
In partial fulfillment of the
Requirements for the degree of
Master of Science in Electrical Engineering

In
The Department of Electrical Engineering

By
Sunil Kumar Challa
B.Tech, J.N.T.U, 2003
August, 2006

ACKNOWLEDGEMENTS

I would like to thank my father, Venkata Naidu Challa, my mother, Durgabai Challa, and my sister Sunitha for their encouragement and enduring patience as well as love and support during the course of my graduate studies.

I would like to express my deepest gratitude to my advisor and teacher, Dr. Ernest Mendrela for the tremendous amount of guidance and support that he provided during the preparation of this dissertation and throughout my entire graduate study.

In addition, I am very grateful to Dr.Leszek S. Czarnecki and Dr. Wu for being members of my committee. I would also like to thank Dr. Dubrako Justic.

TABLE OF CONTENTS

LIST OF TABLES

LIST OF FIGURES

ABSTRACT

The object of the study is a double-sided axial flux permanent magnet brushless dc (AFPM BLDC) motor with salient pole stator. Its winding can be connected either in single-phase or in two-phase system, which results in different operation of the motor

The objective of the thesis is to analyze and compare the performances of the AFPM BLDC motor with single-phase winding and two-phase winding. To study the motor operation, a mathematical dynamic model has been proposed for each of the motor with different winding, which became the basis for simulations that were performed using MATLAB/SIMULINK software package.

The calculations were done for the particular motor which was designed as a water pump with the wet rotor. The results of simulations were presented in form of the waveforms of selected quantities and the electromechanical characteristics performed by the motor in steady-state conditions. The later were the basis for developing a simple mathematical model of the motors which allow to analyze their performance only in steady-state conditions.

. The calculation results show that the two-phase motor version develops more smooth torque and reaches higher efficiency than the single-phase version. However the advantage of using a single-phase version is simpler and cheaper converter which the motor is supplied from. This implicates of using this type of motor for fans and pumps where torque ripple is not the subject, while the two-phase motor can be applied where more smooth torque is required.

Both motors are supplied from inverter whose structure depends on the type of winding. Since there were voltage type inverters, the switching angle of transistors had significance on the motor performance. This influence was studied for both motors

A study on the influence of switching angle on motor performance shows that the motors operate better when advance switching angle $\beta=-30^0$, where the motors operate with the highest efficiency.

CHAPTER 1 INTRODUCTION

Conventional DC motors are highly efficient, however, their only drawback is that they need a commutator and brushes which are subject to wear and require maintenance. The above mentioned deficiency of the conventional solution can be overcome by the new type of DC drive based on brushless DC motors operating without mechanical transmission [1].

The brushless DC motors (Figure. 1.1) are permanent magnet motors where the functions of commutator and brushes were implemented by solid state switches [2]. The brushless DC motors are distinguished not only by the high efficiency but also by their no maintenance. The permanent magnet motors used in this case are single phase or poly phase motors. When operating with single phase or poly phase motors, the inverter plays the role of the commutator. In this project single-phase and two-phase inverters are considered.

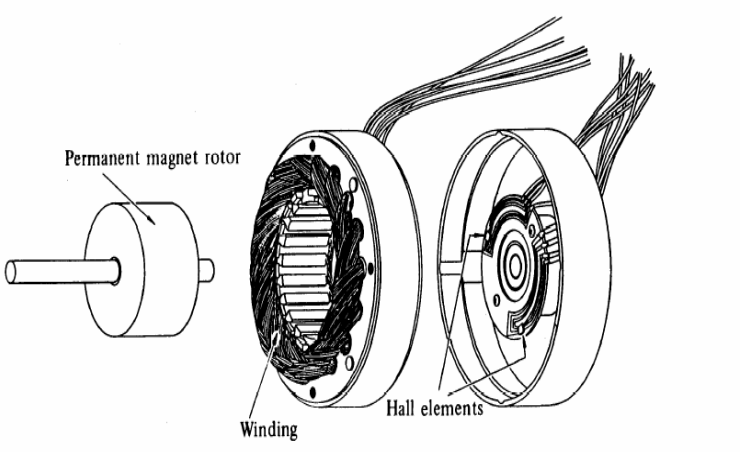

Figure 1.1Permanent magnet brushless DC motor [1]

As far as rotary motor geometry is concerned two types of structures are met: cylindrical and disc structure. In this project a disc motor is considered. According to [3]

the topologies of disc motors, called also axial flux permanent magnet .AFPM machines may be classified as follows:

- Single-sided AFPM machines
    - with slotted stator
    - with slotless stator
    - with salient-pole stator
- Double-sided AFPM machines
    - with internal stator
        * with slotted stator
        * with slotless stator
            .with iron core stator
            .with coreless stator
            .without both rotor and stator cores
        * with salient pole stator
    - with internal rotor
        * with slotted stator
        * with slotless stator
        * with salient pole stator

The object of study in this project is double-sided AFPM brushless machine with internal salient-pole stator and two external rotors shown schematically in Figure.1.2. The stator coils of the motor can be connected in single-phase or poly-phase systems.

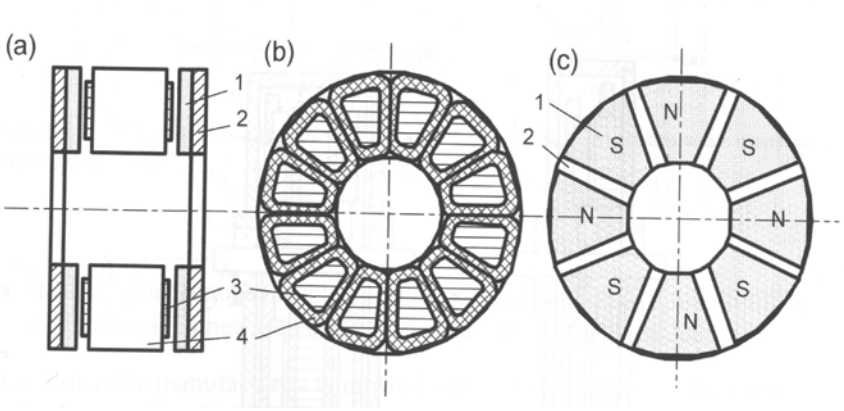

Figure 1.2 Double-sided AFPM brushless machine with internal salient-pole stator and twin external rotor (a) construction,(b) stator (c) rotor, 1-pm, 2-rotor steel disc, 3- stator pole,4-stator coil

These connections imply the single-phase or poly-phase inverters which supply the winding. The type of winding influences the performance of the motor. In this project the performance of the AFPM motor with single-phase and two-phase connections of the stator coils are studied and compared. The particular motor that is analyzed was described in [3]. So far only single-phase and three-phase motors were considered and no comparison study for single-phase and two-phase has been done.

The **objectives** of the project are:

- To study the dynamics of the single-phase and two-phase motors
- To determine the performance of the motor in steady state conditions.

The **tasks** to be accomplished in this project are:

- Literature study on disc brushless DC motors.
- Formulation of the mathematical dynamic models of the motors with single-phase and two- phase windings and simulation of operation on PC.
- Determination of parameters of the steady-state models.
- Calculations of motor performance under variable load conditions.

- Calculations of AFPM motor performance under different switching conditions.
- Comparison of the simulation results of single- phase and two- phase motor.

Outline of thesis

- **Chapter 2** gives literature study on AFPM motor and shows the description of the motor structure and winding diagrams and presents the design data of the motor under study.
- **Chapter 3** contains**:**

  - modeling of single-phase AFPM motor operating in dynamic conditions.

  -computational model of the source inverter-motor set

  -simulation results developed in MATLAB/SIMULINK under different load conditions
- **Chapter 4** contains similar material but it concerns the AFPM motor with two-phase winding.
- **Chapter 5** focuses on modeling of AFPM motor with single-phase and two-phase winding operating in steady-state conditions. The following tasks are considered.
  - formulation of computational model of the motor and determination of its parameters on the basis of the results obtained from the modeling in MATLAB/SIMULINK.
  - study of influence of inverter switching conditions on motor output power and its efficiency.
- **Chapter 6** contains the comparative study of motor performance operating in single-phase and two-phase system and key conclusions.

CHAPTER 2 DESCRIPTION OF MOTOR AND ITS DESIGN DATA

2.1 Literature Review on Axial Flux Permanent Magnet Motors

The history of electrical machines shows that the first machines were – more or less – realized in a form of the axial-flux machine. The first one was invented by Faraday in 1831 and was practically a primitive permanent-magnet DC machine. Radial-flux machines were invented later and were patented firstly by Davenport in 1837. Since then radial-flux machines have dominated excessively the markets of the electrical machines. The first attempts to enter the industrial motor market with radial-flux PMSMs in the 1980's was made by the former BBC, which produced line-start motors with SmCo-magnets[4,5].

The main idea in the early stage of the PMSMs was to increase the efficiency of the traditional electric motors by permanent magnet excitation. However, the efficiency increase was not enough for the customers and the attempts to enter the market failed. Despite of this setback, several manufacturers introduced permanent-magnet machines successfully during the latest decade.

Regardless of the success of radial-flux permanent-magnet machines, axial-flux permanent magnet machines, where the magnetic flux is directed axially in the air-gap and in the stator winding zone and it turns its direction in the stator and rotor core, have also been under research interest particularly due to special-application limited geometrical considerations. A possibility to obtain a very neat axial length for the machine makes axial-flux machines very attractive into applications in which the axial length of the machine is a limiting design parameter. Such applications are, for example,

electrical vehicles wheel motors and elevator motors. Axial flux machines have usually been used in integrated high-torque applications.

AFPM motors can be designed as double sided or single sided machines, with or without armature slots, with internal or external rotors and with surface mounted or interior type permanent magnets (PMs). Low power AFPM machines are usually machines with slotless windings and the surface mounted PMs. Rotors are embedded in power transmission components to optimize the volume, mass, power transfer and assembly time [6].

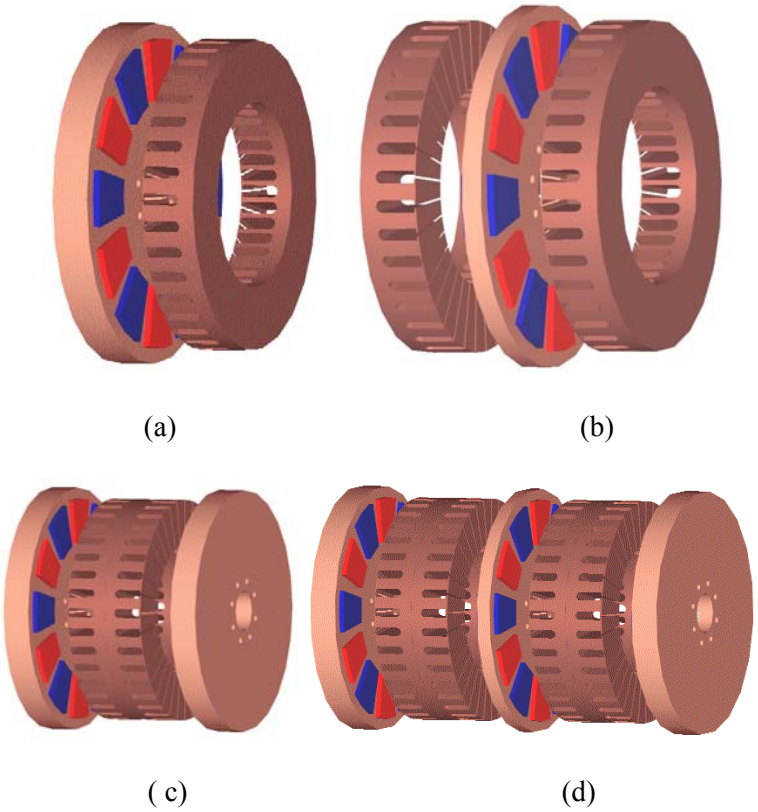

Figure 2.1a. Single-sided AFPM motor, b. double-sided AFPM motor with internal rotor, c. double-sided AFPM motor with external rotors, d. multi stack AFPM motors [4].

Double-sided motor with internal PM disc rotor has the armature windings located on the two stator cores. The disc with the PM rotates between the two stators.

PMs are embedded or glued in a non ferromagnetic rotor skeleton. When the stators are connected in parallel the motor can operate even when one stator windings break down. The stator cores are wounded from electro technical steel strips and the slots are machined by shaping or planning [7, 8].

Several axial-flux machine configurations can be found regarding the stator(s) position with respect to the rotor(s) positions and the winding arrangements giving freedoms to select the most suitable machine structure into the considered application. Possible configurations are shown in Figure. 2.1.

Another common type of AFPM motor is torus type motor which has found numerous applications, in particular, in gearless drives for electrical vehicles. It resembles the motor shown in Figure.2.1.c. The stator however has slotless core and the Gramme' s type winding [6, 13]. The stator core is made of laminated iron. The rotor discs are made of solid iron contain the high energy permanent magnets glued to their surfaces.

2.2 Axial Flux Permanent Magnet Motor Structure

Double-sided AFPM motor with one stator, which is an object of this study, is shown in Figure. 2.2 [8, 12]. It is more compact than the motor with internal rotor. The double-sided rotor with PMs is located at the two sides of the stator. The stator consists of the electromagnetic elements made of ferromagnetic cores and coils wound on them. These elements are placed axially and uniformly distributed on the stator circumference and glued together by means of synthetic resin.The particular motor with the dimensions shown in Figure. 2.3 was designed as an integrated water pump [8]. The stator coils can be connected in single-phase and multi-phase systems. The motor of particular winding

connection exhibits its unique performance that differs it from the motors of the other connection systems. In this project motor with single-phase and two-phase are studied and are analyzed and compared.

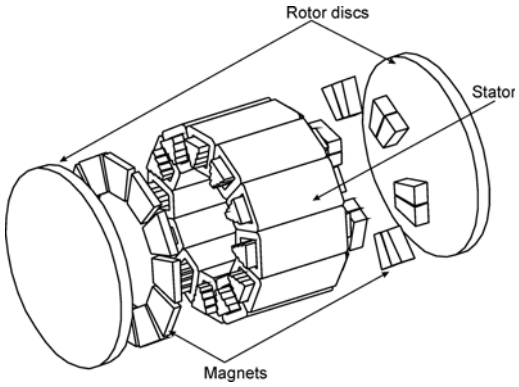

Figure 2.2 Scheme of double sided motor with one stator is considered in this project [12]

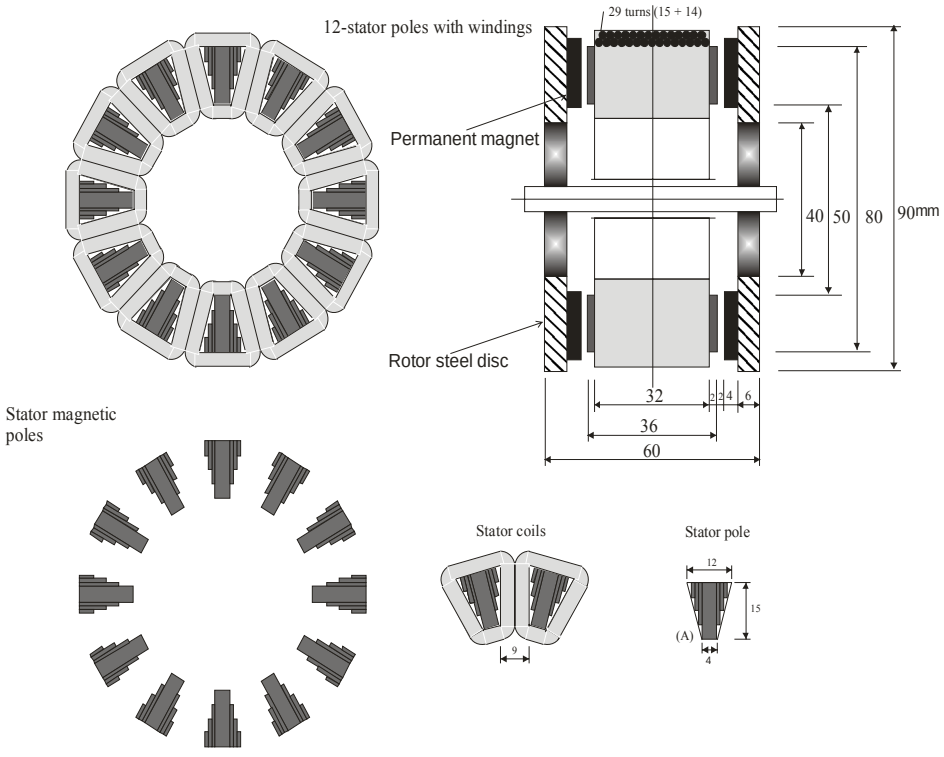

Figure 2.3 Scheme of AFPM motor with internal salient pole stator [8]

On both sides of the stator are the rotors made of steel discs with the permanent magnets glued to the disc surfaces [5, 6] .The distribution of the magnets on the rotor discs has to be adequate to the stator poles polarity and as for single-phase motor is shown in Figure. 2.4.

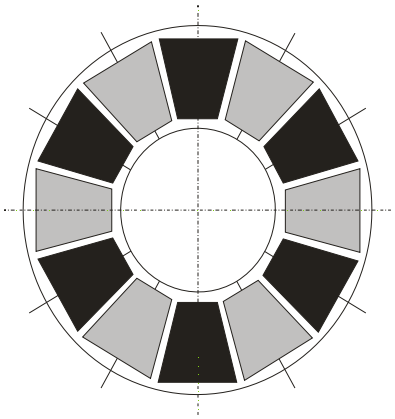

Figure 2.4 Configuration of PMs on the rotor disc for a single phase winding [8]

2.3 AFPM Brushless Motor with Single - Phase Winding

The windings of the stator (Figure.2.5) of AFPM brushless motor in the single phase connection are shown in Figure. 2.6.a. Here the coils 1 to 6 and 7 to 12 are connected in series and both these series connections are connected in parallel as shown in the Figure. 2.6.b.

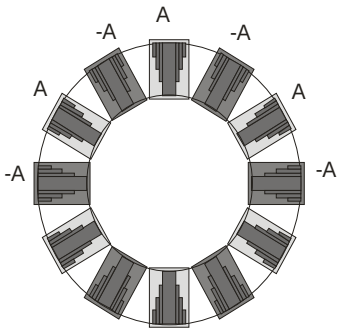

Figure 2.5 Distribution of stator poles and rotor PMs for single-phase motor [7]

The windings of the stator (Figure.2.5) of AFPM brushless motor in the single phase connection are shown in Figure. 2.6.a. Here the coils 1 to 6 and 7 to 12 are connected in series and both these series connections are connected in parallel as shown in the Figure. 2.6. b.

(a) (b)

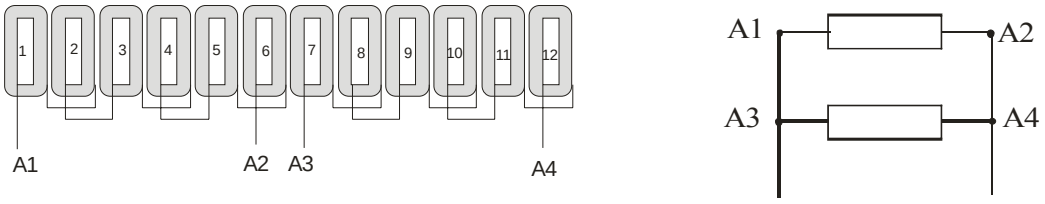

Figure 2.6 Windings of the stator connected [8].

The inverter considered for the AFPM brushless motor with single-phase winding is shown in the Figure. 2.7. It alternates the polarity of the stator current and it is also called electronic commutator. It is an H-type dc to ac converter operating within the feed back control loop. Transistors pairs T1, T4 and T2, T4are switched on accordingly depending on the rotor position. The voltage v_{sa} from the inverter that supplies the motor is a square waveform shown in Figure 2.8 and is a function of rotor position.

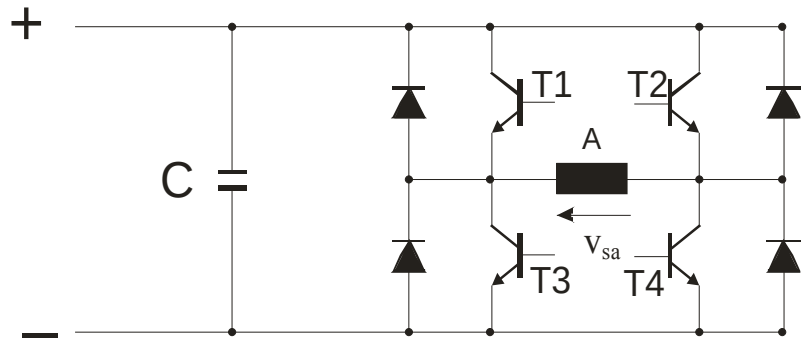

Figure 2.7 Inverter for AFPM brushless motor with single-phase winding [8]

Normally, the supply voltage v_{sa} is in phase with electromotive force e_a induced in the winding. The switching angle between v_{sa} and e_a may be changed to improve the performance of the motor. This is discussed in Chapter 5. The position sensors are placed between the coils in the intervals of 180^0.These sensors sense the position of the rotor and they trigger the transistors so that they switch on and off the stator winding.

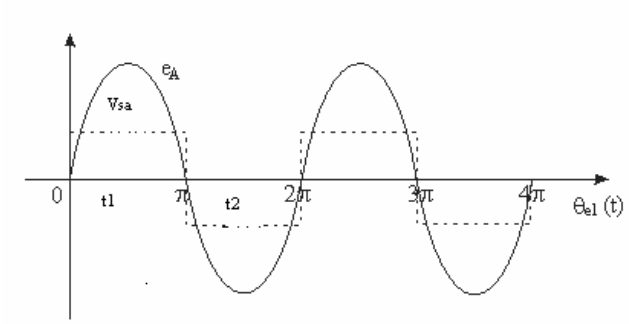

Figure 2.8 Waveforms of supply voltage v_{sa} and back electromotive force e_a

At an instant t_1 transistor T1 and T4 (Figure. 2.9.a.) are switched on and the rotor takes the position with respect to the stator as in Figure. 2.9.b.

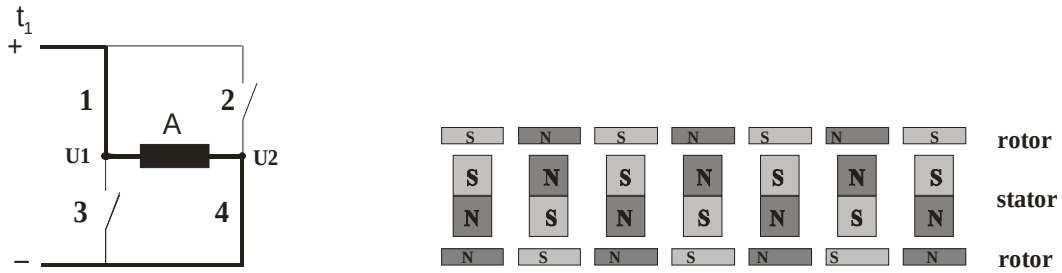

(a) (b)

Figure 2.9 a. At t_1T1 and T4 switched ON, b. Mutual position of stator and rotor magnetic poles at instant t_1

At instant t_2 transistors T2 and T3 are triggered on in (Figure. 2.11. a.) and the mutual position of stator and rotor is as shown in Figure. 2.11.b.

The above AFPM motor has the same number of rotor magnets as the magnetic poles in the stator. This contributes to the rise of cogging torque. Due to that the position of the rotor magnets with regard to the stator poles, when the winding is switched off, is as shown in Figure. 2.9.b. Now, when the winding is switched on the stator does not move because the motor does not develop any starting torque. To make it moves the magnets on one of the rotor discs should be rearranged in the way as shown in Figure. 2.12.

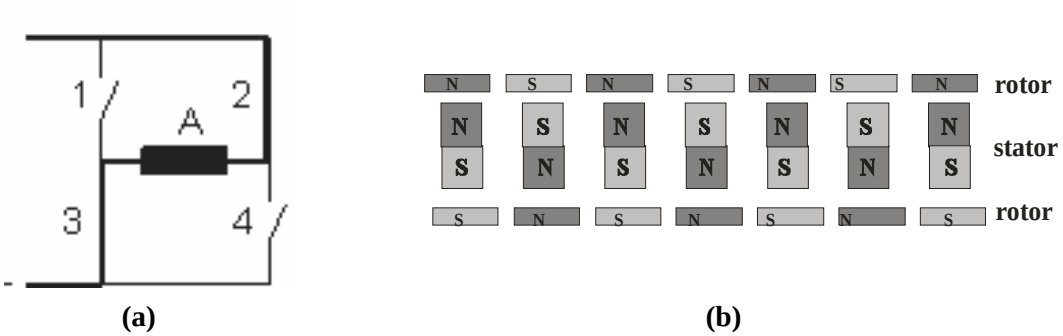

Figure 2.10 a. At t_2 T1 and T4 switched ON, b. Mutual position of stator and rotor magnetic poles at instant t_2

Figure.2.12 illustrates the variation of the electromagnetic torque versus rotational angle. When the motor is switched off the rotor is at detent position. If we move the rotor in relation to the stator, which is now switched on, and a polarity of its poles does not change and is as shown in Figure.2.12, the rotor experiences the torque coming from the small magnets as show the curves **n** and **s**. Curve **NS** illustrates the variation of the torque developed by the magnets **N** and **S** is the **NS + sn** characteristic.The resultant torque experienced by the rotor

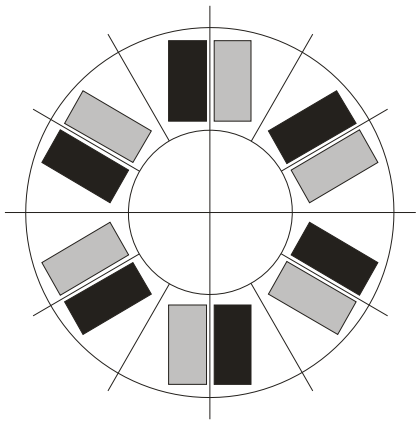

Figure 2.11 Rearranged magnets on one of the rotor disc [8].

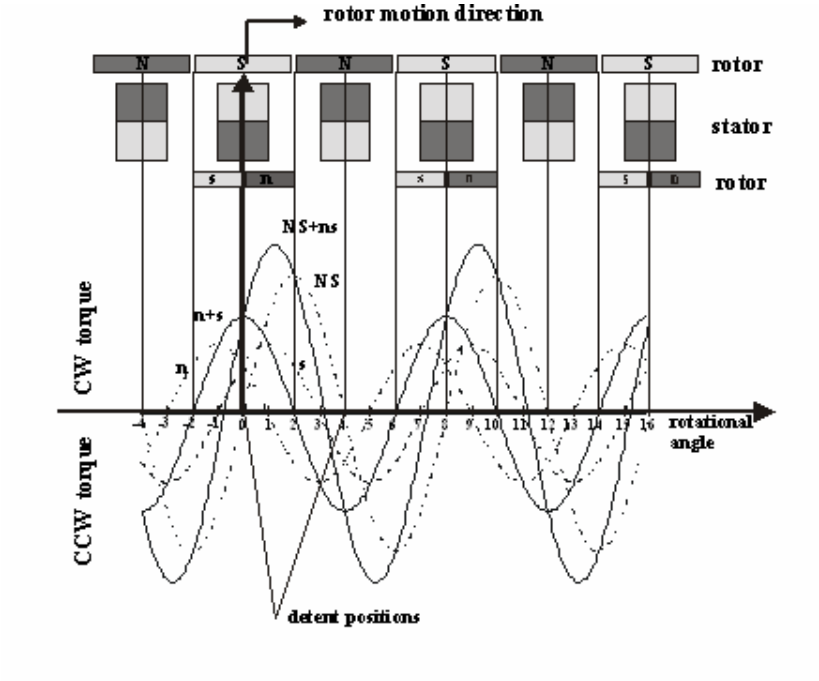

Figure 2.12 Torque components developed at constant armature current in single phase motor [8].

As one can see there is a starting torque now at detent position. This torque should overcome the load torque and the detent torque (cogging torque) created by the salient poles of the stator as well. Curve **NS + ns** show the torque at steady stator polarity. Due to the electronic commutator the polarity alternates and there is always positive torque acting on the rotor.

In order to produce the starting torque in the brushless dc motor with the single-phase winding other methods can be used. One of them is to add to the stator the auxiliary salient poles placed between the existing electromagnetic poles. The other way is to apply the rotor with the magnet structure, which is a combination of two parts of magnets, where one has the double number of poles than another.

2.4 AFPM Brushless Motor with Two - Phase Winding

The stator (Figure 2.14) winding in this case is connected as shown in Figure. 2.15. Here the coils of phases A and B are alternatively connected. The inverter considered for the AFPM brushless motor with two- phase winding is shown in Figure. 2.16.

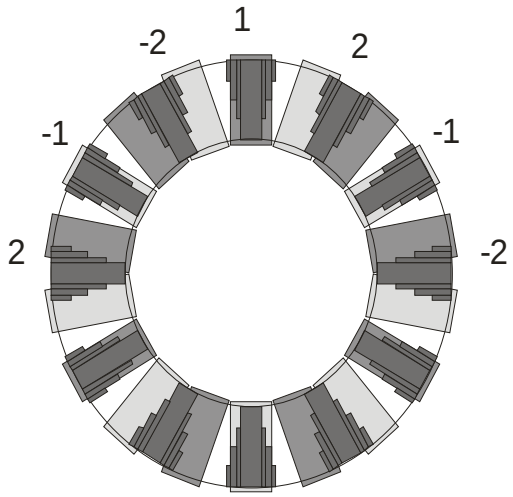

Figure 2.13 Distribution of stator and rotor magnetic poles for AFPM with Two-Phase winding [11]

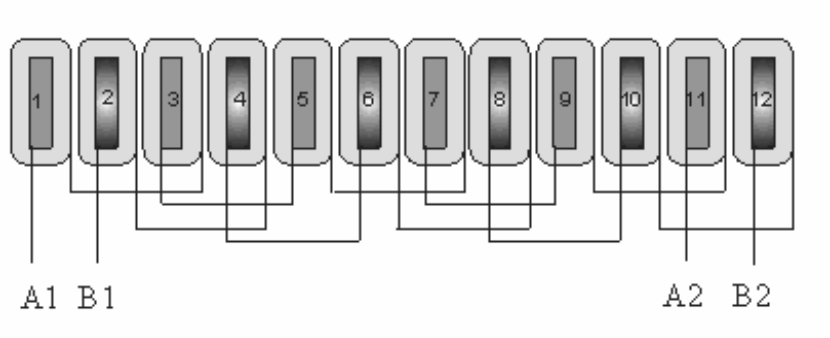

Figure 2.14 Windings of the stator is connected in Two - phase

The position sensors are placed between the coils in the intervals of 90^0 .These sensors sense the position of the rotor and they trigger the transistors so that they switch on the respective stator winding.

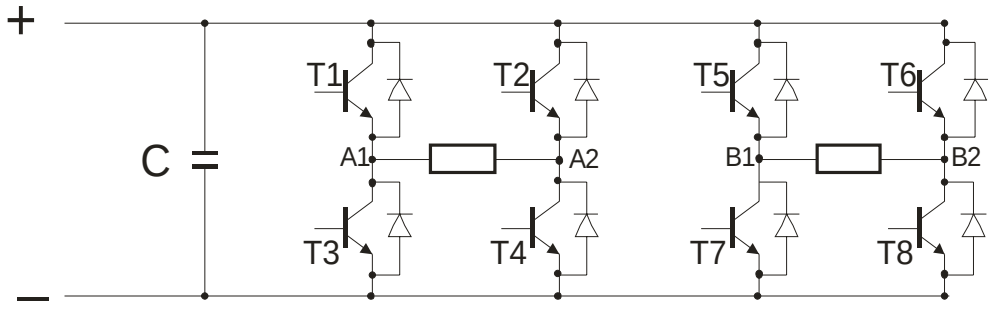

Figure 2.15 Inverter considered for AFPM with Two-Phase Winding

Same as in single-phase case, the voltage v_{sa} , v_{sb} from the inverter that supplies the motor are square waveforms shown in Figure 2.17 and are the functions of rotor position. They are normally in phase with their appropriate magnetic forces e_a and e_b induced in the phase windings A and B. These voltages v_{sa} and v_{sb} can be displaced in time when the switching angle in order to improve the motor performance. This will be discussed in Chapter 5, section 5.2.

Figure. 2.17 and 2.18 show the operation of the motor. At instant t_1 transistors T1 and T4 are triggered on (Figure. 2.17.a) and the mutual position of stator and rotor is as shown in Figure 2.17.b.

When the rotor rotates 90^0 of electrical angle at the instant t_2 transistors T5 and T8 are triggered [Figure 2.18 a] and the mutual position of stator and rotor is as shown in Figure 2.18 b.

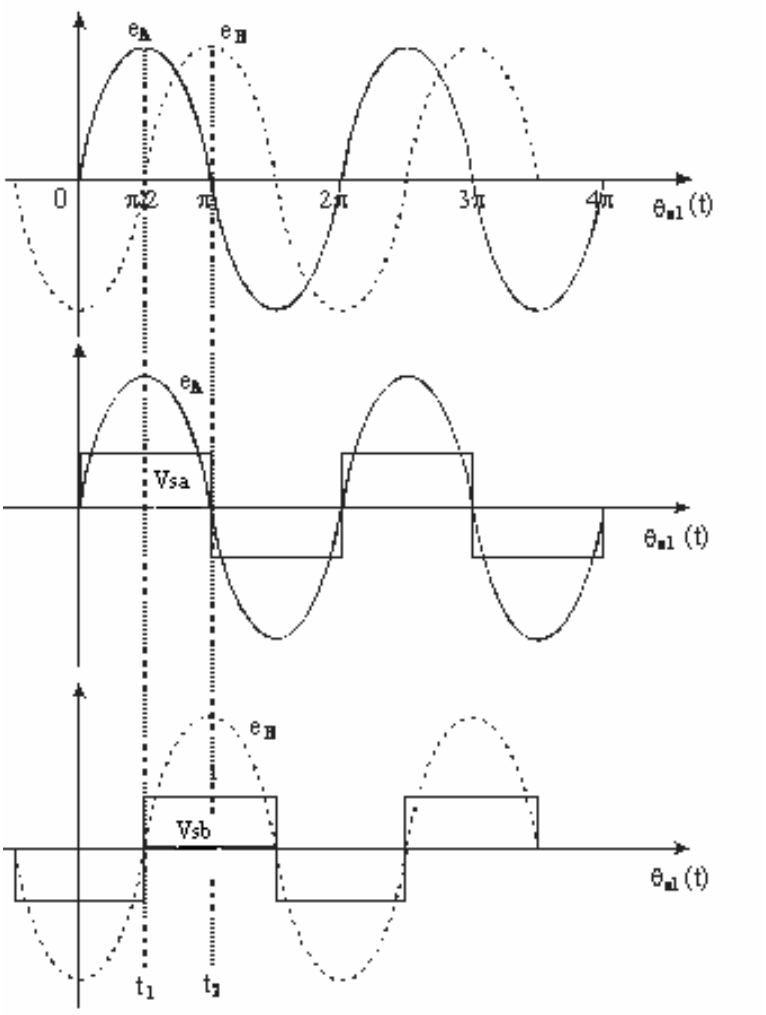

Figure 2.16 waveforms of supply voltage v_{sa} and v_{sb} and electromotive forces induced in two-phase winding

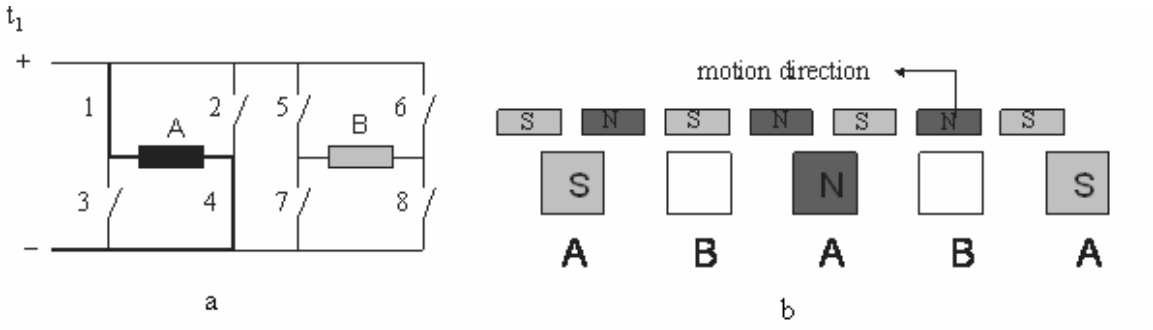

Figure 2.17.a At t_1 T1 and T4 switched ON, b. Mutual position of stator and rotor magnetic poles at instant t_1

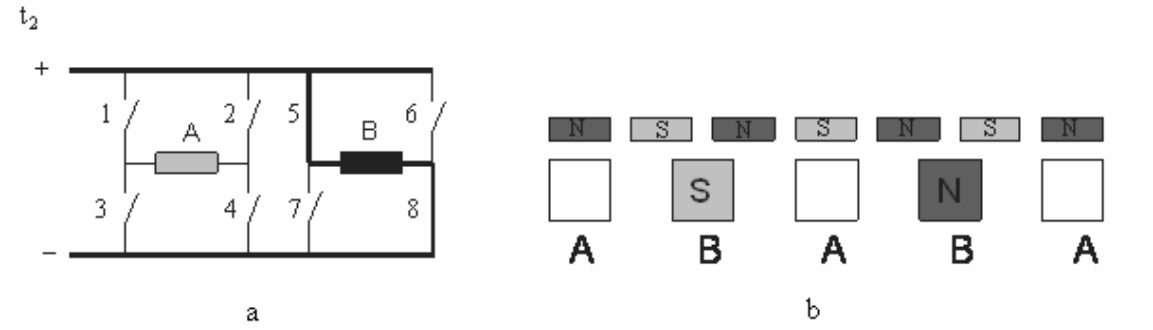

Figure 2.18.a At t_2 T5 and T8 switched ON, b. mutual position of stator and rotor magnetic poles at instant t_2

CHAPTER 3 DYNAMIC OF SIMULATION OF AFPM BRUSHLESS MOTOR WITH SINGLE PHASE WINDING

3.1 Dynamic Model of the Single Phase Motor

The supply-inverter-motor circuit model is shown in Figure.3.1. The circuit parameters are set up under the following assumptions:

- All elements of the motor are linear and no core losses are considered,
- Electromotive force e_a and cogging torque vary sinusoidally with the rotational electric angle θ_e
- Due to the surface mounted permanent magnets winding inductance is constant (does not change with the θ_e angle),
- Voltage drops across diodes and transistors and connecting wire inductance are ignored.

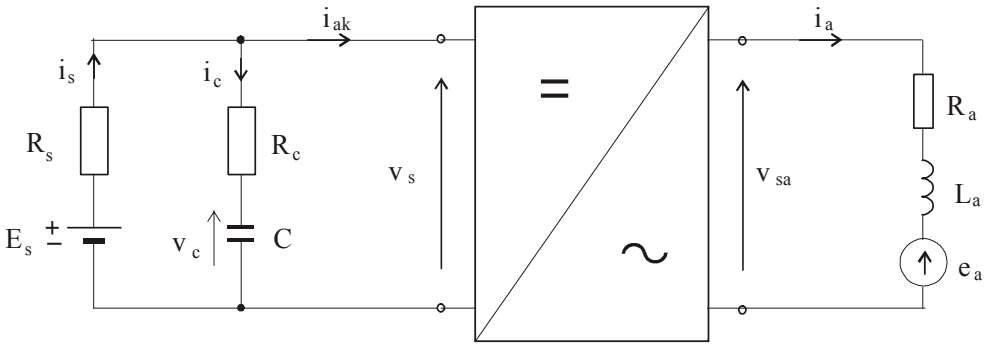

Figure 3.1 Circuit diagram of supply-inverter-motor

The voltage equations that describe the model are as follows:

- Voltage equation at the supply side

$$E_s - i_s R_s - i_c R_c - v_c = 0 \tag{3.1}$$

$$v_s = v_c + i_c \cdot R_c \tag{3.2}$$

$$i_s = i_{ak} + i_c \tag{3.3}$$

where:

E_s and R_s – voltage and resistance of the source

R_c – capacitor resistance

i_s – source circuit current

i_{ak} – converter input current

v_c – voltage across capacitor

$$v_c = \frac{Q_c}{C} \tag{3.4}$$

Q_c – charge in capacitor

C – capacitance

i_c – current flowing through the capacitor:

$$i_c = \frac{dQ_c}{dt} \tag{3.5}$$

- Voltage equation at the motor side:

$$v_{sa} = R_a i_a + L_a \frac{di_a}{dt} + e_a \tag{3.6}$$

The voltage v_{sa} that supplies the motor is a square wave (see Figure 2.1) and is a function of rotor position which is generated by the position sensor. So, it is described by the function.

$$v_{sa} = sign[\sin(\theta_e + \alpha)]v_s \tag{3.7}$$

Thus the voltage equation is:

$$sign[\sin(\theta_e + \alpha)]v_s = R_a i_a + L_a \frac{di_a}{dt} + e_a \tag{3.8}$$

Due to the equality of the converter input and output powers (no power losses in the converter are assumed):

$$v_s i_{ak} = v_{sa} i_a \tag{3.9}$$

We have:

$$i_{ak} = \frac{v_{sa}}{v_s} i_a \tag{3.10}$$

The electromotive force induced in the winding (see Figure 3.2):

$$e_a = K_E \omega_m \sin(\theta_e) \tag{3.11}$$

where:

K_E – constant

ω_m – rotor angular speed:

$$\omega_m = \frac{1}{p} \frac{d\theta_e}{dt} \tag{3.12}$$

θ_e – Electrical angle (Figure. 3.2)

p – Number of pole pairs

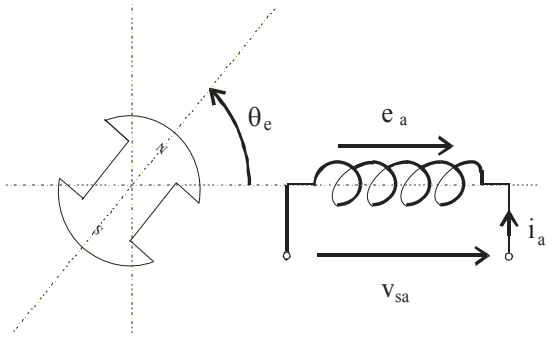

Figure 3.2 Calculation model of single-phase motor

The mechanical system with all torques is shown schematically in Figure. 3.3. This system

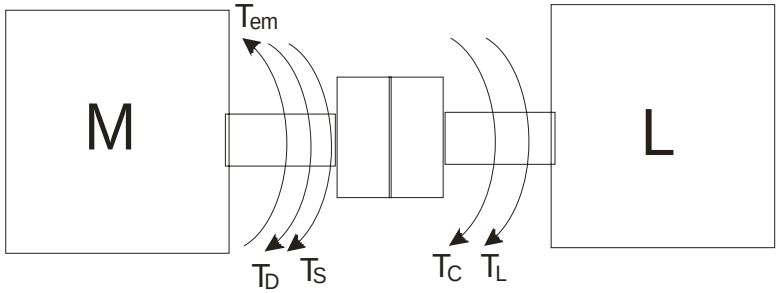

Figure 3.3 Mechanical system with torques

is defined by the following equation 3.13.

$$T_J + T_D + T_s + T_c + T_l = T_{em} \tag{3.13}$$

The torque components of equation 3.13 are expressed by the following equations:

- inertia torque:

$$T_J = J \frac{d\omega_m}{dt} \tag{3.14}$$

- viscous friction torque:

$$T_D = D \cdot \omega_r \tag{3.15}$$

- coulomb friction torque:

$$T_s = sign(\omega_r) T_d \tag{3.16}$$

- cogging torque:

$$T_c = T_{mc} \sin(2\varphi_e + \beta) \tag{3.17}$$

- load torque: T_l

- electromagnetic torque:

$$T_{em} = \frac{e_a i_a}{\omega_m} = \frac{K_E \omega_m \sin\theta}{\omega_m} i_a = K_E i_a \sin\theta \tag{3.18}$$

Other symbols used in above equations are:

J – moment of inertia

D – friction coefficient

T_{mc} – cogging torque amplitude

β – displacement angle of cogging torque

3.2 Parameters of Electric Circuit and Mechanical System

Calculations of motor performance were carried out for the system parameters presented in Table 3.1.

Table 3.1Parameters of electric circuit and mechanical system

$E_b = 300\ V$	emf of the battery
$R_s = 1.5\ \Omega$	source resistance
$R_c = 2\ \Omega$	resistance in series with capacitor
$C = 10\ \mu F$	capacitance
$R_a = 8\ \Omega$	phase resistance of the brushless DC motor
$L_c = 0.042$ H	phase resistance of the brushless DC motor
$K_e = 1.324$	emf constant
$J = 0.001\ Kg/m^2$	moment of inertia
$D = 0.001$ N/(rad/s)	friction coefficient

$T_{load} = 2.2 N.m$	load torque
$T_s = 0.1 N.m$	coulomb friction torque

3.3 Dynamic Simulation of the Motor

The simulation of the motor operation in dynamic conditions is done by using MATLAB/SIMULINK software version 7.0.

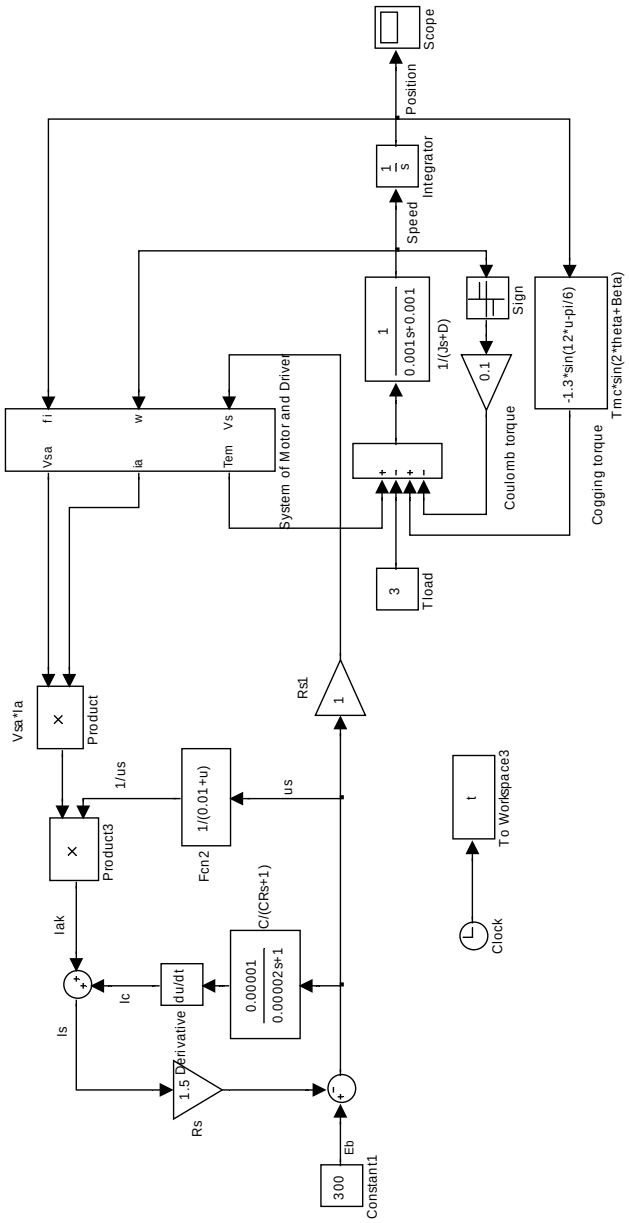

Figure 3.4 Simulink Block of AFPM motor with single phase winding

The simulation block diagram which is shown in Figure 3.3 implements the basic equations that describe the fully operation of the system. It consists of three parts: supply voltage, inverter and motor winding and mechanical system of the drive. It also consists of subsystem related to the inverter and motor winding which is shown in Figure 3.4. In

this diagram the electromotive force e_A is generated by the rotor position signal θ_e and the appropriate function $f_a(\theta_e)$.

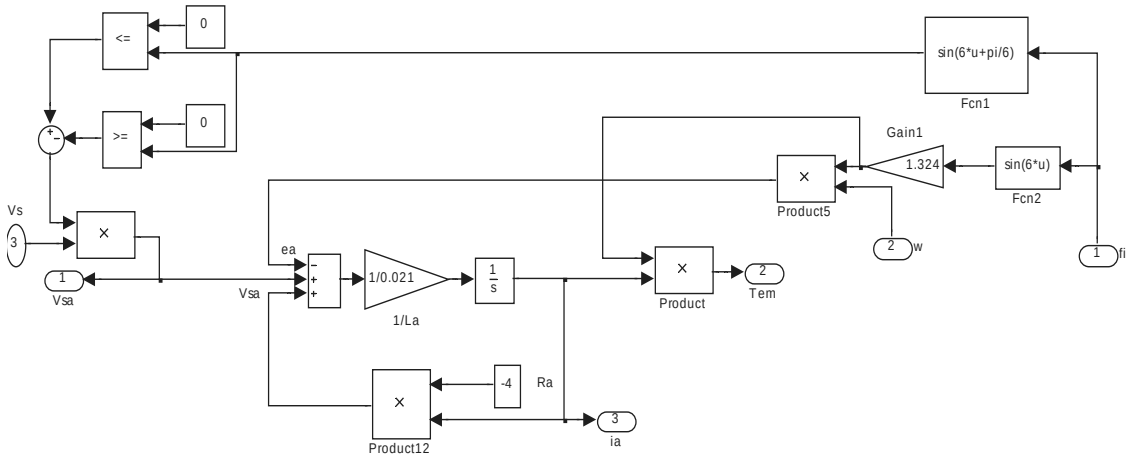

Figure 3.5 Simulink Model of Inverter-motor Circuit subsystem

3.3.1 Starting up Operation

To simulate this operation, it was assumed that the drive system is supplied with constant voltage of 300 V, and the system was loaded with the rated torque of 2.2 N.m and the Switching angle is -30^0.

The simulation results are shown in Figs 3.5, 3.6, 3.7, 3.8 and 3.9. In particular the Figure. 3.5 shows the rotary speed (n) and source current (i_s) waveforms. The ripple in the speed waveform is due to the oscillation of the motor torque. It consists of two components: electromagnetic torque T_{em} and cogging torque T_c. These two torque components are shown in Figure. 3.9, which were drawn when the motor reached steady-state. The electromagnetic torque waveform during the starting process is shown in Figure 3.8. The results presented in Figure 3.9 show that the torque developed by the motor is always positive despite the relatively big cogging torque components. As has

been written in Chapter 2, this positive resultant torque is obtained due to displacement of PMs on one of the rotor discs.

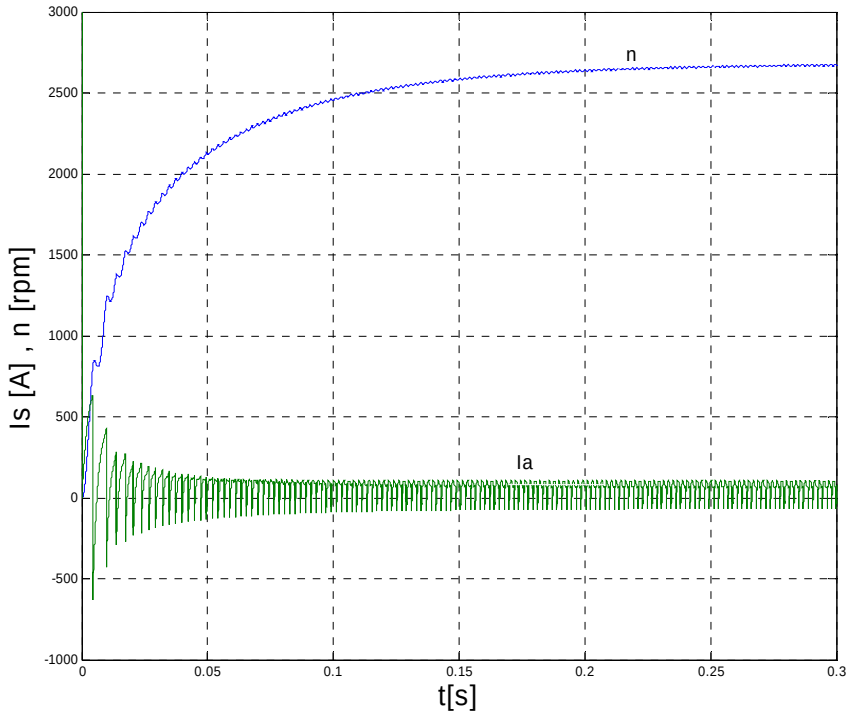

Figure 3.6 Waveform of rotary speed (n) and source current (i_s)

The waveforms of EMF (e_a) and armature voltage (v_a) are shown in Figure 3.6. The induced EMF and the voltage applied to the motor are in phase because the winding was switched ON without any delay with respect to the position of magnets and winding.

Figure 3.7 shows the current and voltage waveforms. The shape of current waveforms is far from being rectangular due to the influence not only by the voltage but by emf and by the winding inductance. The cogging torque (R), electromagnetic torque (T) and the resultant torque (T+R) are shown in the above Figure 3.9

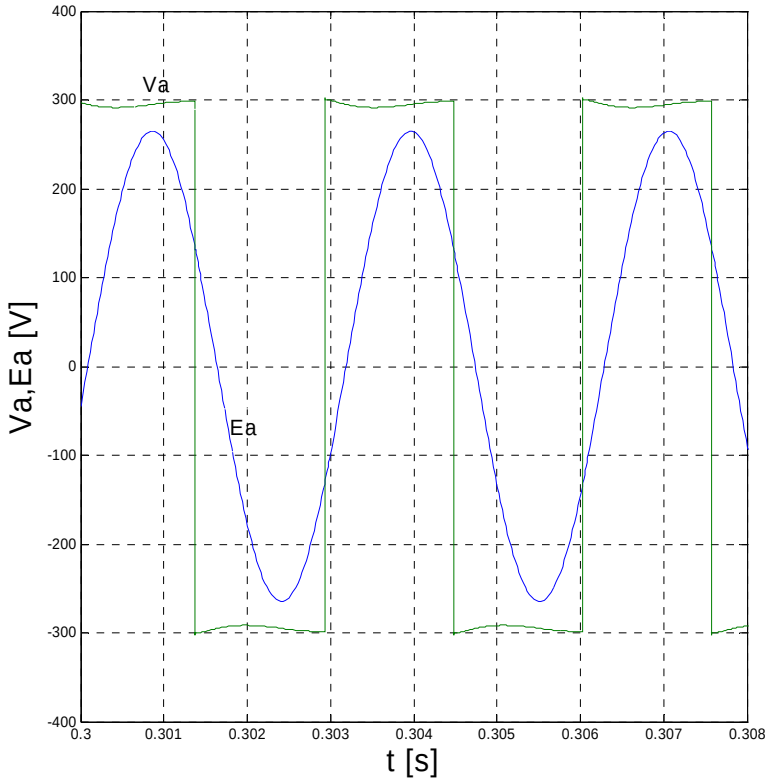

Figure 3.7 Waveform of EMF (e_a) and armature voltage (V_a)

.The motor after starting process reaches the steady-state operation within 1 sec. The motor was loaded with the rated torque of 2.2 N.m. Thus the values of other quantities can be regarded as the rated ones. Their average values were calculated and listed in Table 3.2.

The motor efficiency was calculated as

$$Eff_{\%} = \frac{P_{out}}{P_{in}}.100\% \qquad (3.19)$$

where:

the average input power:

$$P_{in} = \frac{1}{T}\int_0^T (v_s \cdot i_{ak})dt \qquad (3.20)$$

the average output power:

$$P_{out} = \frac{1}{T}\int_0^T (T_L \cdot \omega)dt \tag{3.21}$$

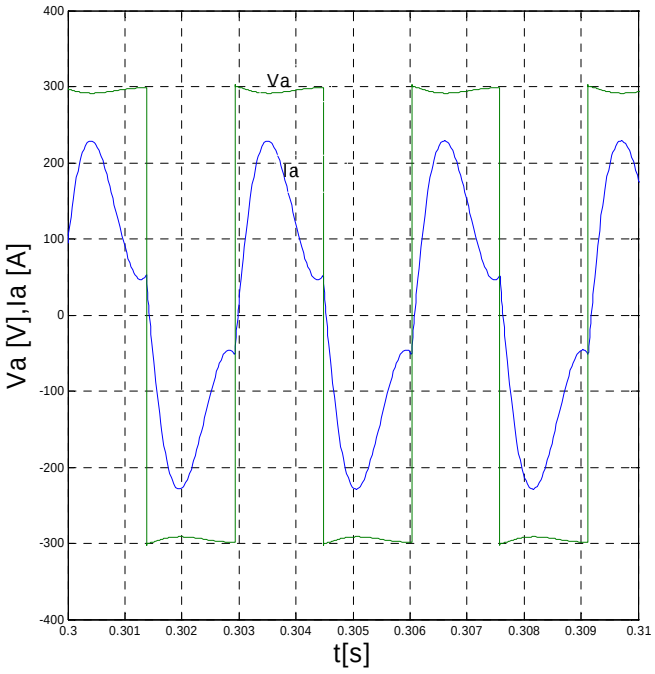

Figure 3.8 Waveform of armature current (i_a) and armature voltage (V_a)

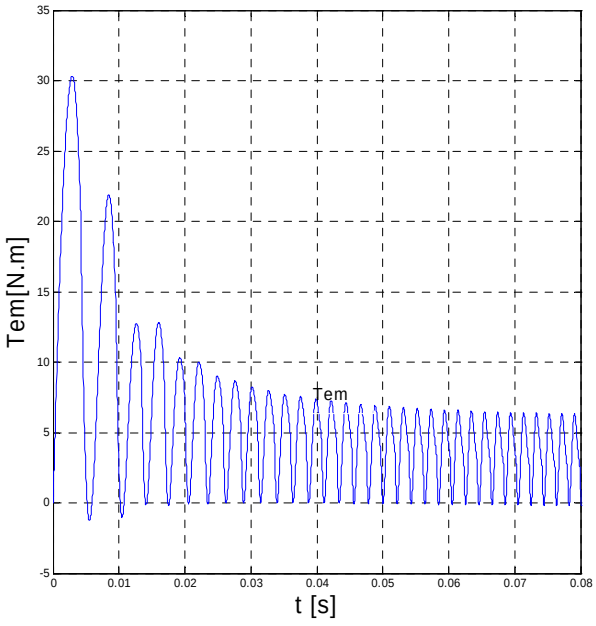

Figure 3.9 Waveform of electromagnetic torque (Tem)

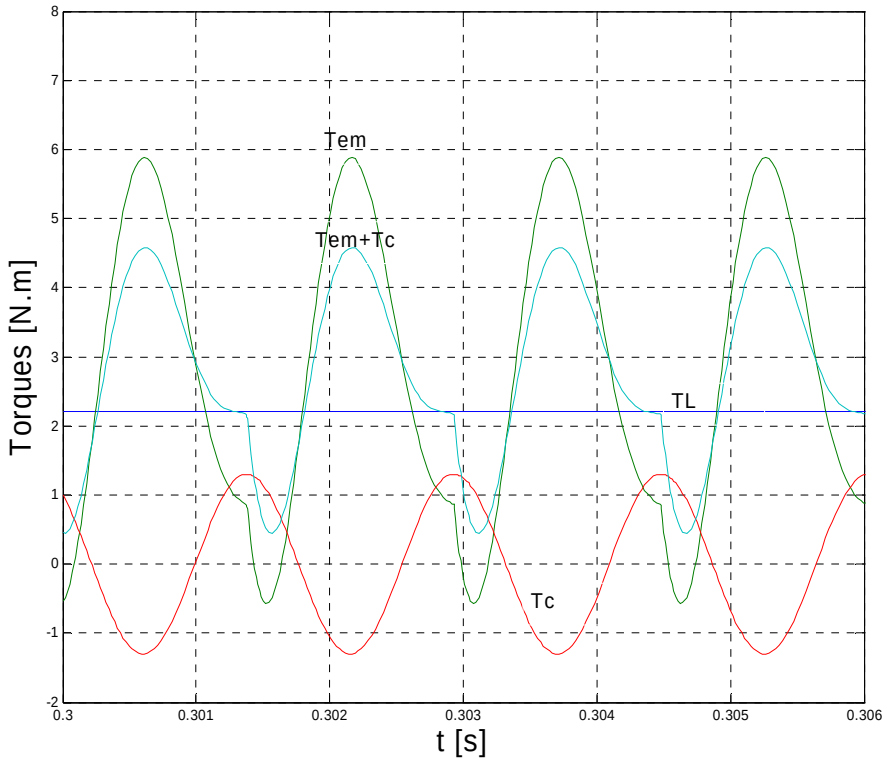

Figure 3.10 Waveforms of electromagnetic torque (T_{em}), cogging torque (T_c), resultant torque ($T_{em} + T_c$)

Table 3.2Average values at rated torque at 2.2 N.m

Supply Voltage	300 *V*
Output Power	756 *W*
Rotary speed	3278 *rpm*
Torque	
Efficiency	2.2 *N.m*
	78.17 *%*

The electromechanical characteristics are plotted for various loads at constant supply 300 V and at switching angle (β) = -30^0 are shown in Figure 3.11

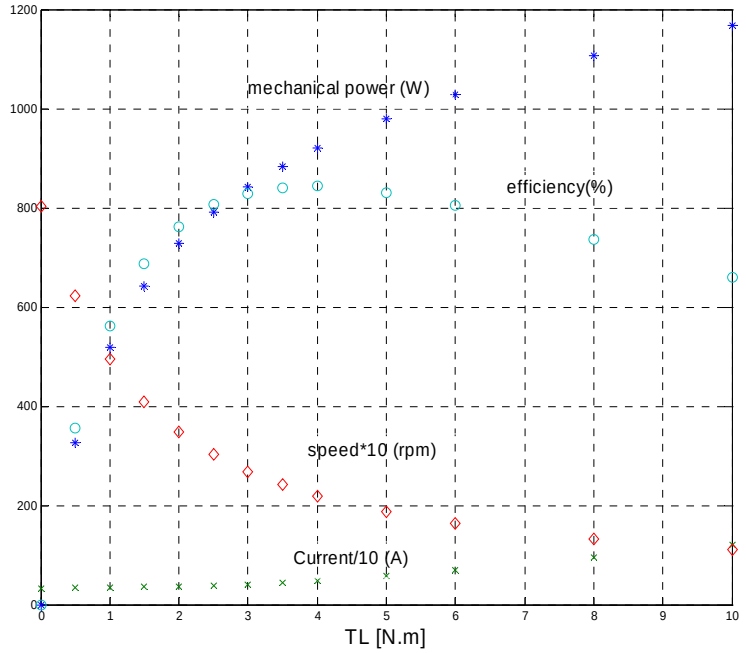

Figure 3.11Electromechanical characteristics of motor at constant supply and β = $--30^0$

CHAPTER 4 SIMULATION OF TWO-PHASE MOTOR DYNAMICS

4.1 Mathematical Model of the Supply–Inverter–Motor System

- The supply-inverter-motor circuit model is shown in Figure 4.1.

The assumptions are similar to that for single phase AFPM brushless DC motor which are stated in section 3.1.

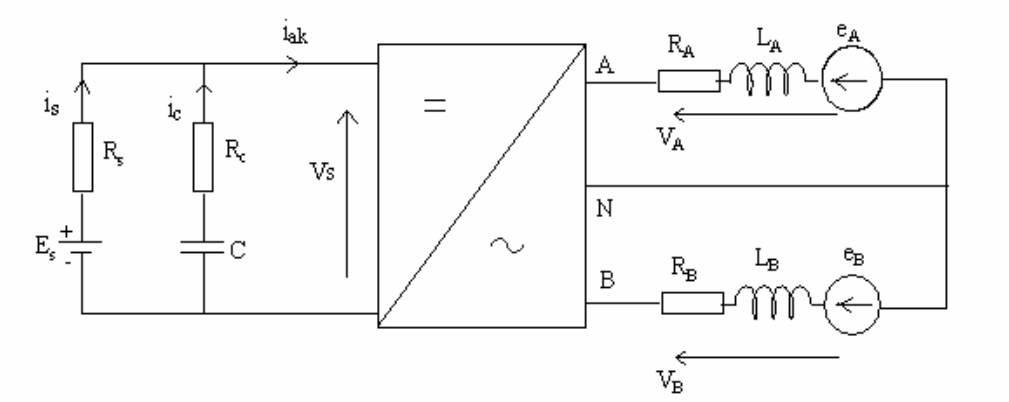

Figure 4.1 Circuit diagram of supply-inverter-motor system

The equations that describe the model are as follows:

Voltage equations

- Voltage equation at the source side:

$$E_b - i_s \cdot R_b - i_c \cdot R_c = 0 \tag{4.1}$$

$$v_s = v_c + i_c \cdot R_c \tag{4.2}$$

$$i_s = i_{sk} + i_c \tag{4.3}$$

where:

E_b and R_b – voltage and resistance of the source

R_c – capacitor resistance

i_s – source circuit current

i_{sk} – converter input current

v_c – voltage across capacitor:

$$v_c = \frac{Q_c}{C} \tag{4.4}$$

Q_c – charge in capacitor

C – capacitance

i_c – current flowing through the capacitor:

$$i_c = \frac{dQ_c}{dt} \tag{4.5}$$

- Voltage equations at the motor side (Figure 4.2) are:

$$v_A = v_{sA} \tag{4.6}$$

$$v_B = v_{sB} \tag{4.7}$$

where:

v_{sA}, v_{sB}, are the inverter output voltages that supply the 2 – phase winding

v_A, v_B, are the voltages across the motor armature winding

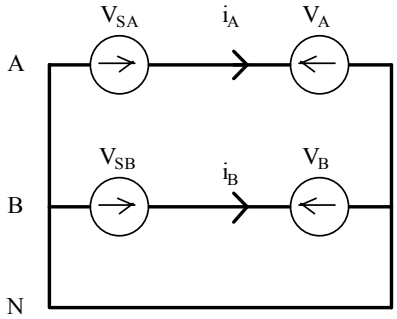

Figure 4.2 Scheme to the equation 4

The equation of the voltages across the motor winding

$$\begin{bmatrix} v_A \\ v_B \end{bmatrix} = \begin{bmatrix} R_a & 0 \\ 0 & R_b \end{bmatrix} \begin{bmatrix} i_A \\ i_B \end{bmatrix} + \frac{d}{dt} \begin{bmatrix} L_A & L_{AB} \\ L_{BA} & L_B \end{bmatrix} \begin{bmatrix} i_A \\ i_B \end{bmatrix} + \begin{bmatrix} e_A \\ e_B \end{bmatrix} \tag{4.8}$$

or in shortened version:

$$\mathbf{V_a} = \mathbf{R_a} \cdot \mathbf{I_a} + \frac{\mathbf{d}}{\mathbf{dt}} \mathbf{L_a} \cdot \mathbf{I_a} + \mathbf{E_a} \tag{4.9}$$

Since the resistances R_a of all phases are the same:

$$\mathbf{R_a} = \begin{bmatrix} R_a & 0 \\ 0 & R_a \end{bmatrix} \tag{4.10}$$

Here there is no mutual inductance between the phases A and B, they are displaced by 90^0. So, $L_{AB}, L_{BA} = 0$.

Due to the symmetrical winding the inductances $L_A = L_B = \mathrm{L}$

The inductance matrix takes the form:

$$L_a = \begin{bmatrix} L & 0 \\ 0 & L \end{bmatrix} \tag{4.11}$$

$$\text{Here} \quad i_a + i_b = 0 \tag{4.12}$$

Thus the voltage equation takes the form:

$$\begin{bmatrix} v_A \\ v_B \end{bmatrix} = \begin{bmatrix} R_A & 0 \\ 0 & R_B \end{bmatrix} \begin{bmatrix} i_A \\ i_B \end{bmatrix} + \frac{d}{dt} \begin{bmatrix} L & 0 \\ 0 & L \end{bmatrix} \begin{bmatrix} i_A \\ i_B \end{bmatrix} + \begin{bmatrix} e_A \\ e_B \end{bmatrix} \tag{4.13}$$

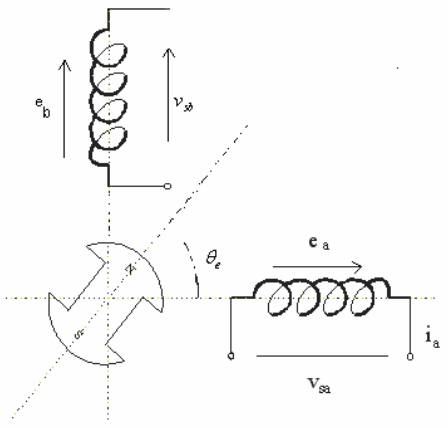

Figure 4.3 Position of the rotor with respect to the phase A

The electromotive force induced in the phase *A* winding (see Figure 6.3):

$$e_a = K_E \omega_m \sin(\theta_e) \tag{4.14}$$

The electromotive force induced in the phase *B* winding is given by

$$e_b = K_E \omega_m \sin(\theta_e - 90^0) \tag{4.15}$$

Where:

K_E – constant

ω_m – rotor angular speed:

$$\omega_m = \frac{1}{p}\frac{d\theta_e}{dt} \tag{4.16}$$

θ_e – electrical angle (Figure 2)

p – number of pole pairs

For three-phase winding, the electromotive forces written in a form of matrix $\boldsymbol{E_a}$

$$\mathbf{E_a} = \frac{K_E}{p}\begin{bmatrix} \sin\theta_e \\ \sin(\theta_e - \frac{\pi}{2}) \end{bmatrix}\frac{d\theta_e}{dt} \tag{4.17}$$

Equation that links the supply and motor sides:

$$i_{sk} = \frac{1}{v_s}(i_A v_{sA} + i_B v_{sB}) \tag{4.18}$$

results from the equality of the powers at input and output of the inverter.

Supply voltages for the phases (v_{sA}, v_{sB}) results from the operation of converter.

Motion equation:

The motion equation is same as for single phase (3.13) case, except that the electromagnetic torque is given by following equations 4.19 and 4.20.

$$T_{em} = \frac{e_A i_A}{\omega_r} + \frac{e_B i_B}{\omega_r} \tag{4.19}$$

$$T_{em} = \frac{e_A i_A}{\omega_R} + \frac{e_B i_B}{\omega_R} = K_E(f_a(\theta_e).i_A + f_b(\theta_e).i_B \tag{4.20}$$

where

$$f_a(\theta_e) = \sin(\theta_e)$$
$$f_b(\theta_e) = \sin(\theta_e - \frac{\pi}{2})$$

Combining all the above equations, the system in steady-space form is [24]

$$\dot{x} = Ax + Bu \tag{4.21}$$

$$x = \begin{bmatrix} i_A & i_B & \omega_r & \theta_e \end{bmatrix}^t \tag{4.22}$$

$$A = \begin{bmatrix} -\frac{R_s}{L} & 0 & -\frac{K_E(f_a(\theta_e))}{L} & 0 \\ 0 & -\frac{R_s}{L} & -\frac{K_E(f_a(\theta_e))}{L} & 0 \\ \frac{K_E(f_a(\theta_e))}{J} & \frac{K_E(f_b(\theta_e))}{J} & -\frac{D}{J} & 0 \\ 0 & 0 & \frac{P}{2} & 0 \end{bmatrix} \tag{4.23}$$

$$B = \begin{bmatrix} \frac{1}{L} & 0 & 0 \\ 0 & \frac{1}{L} & 0 \\ 0 & 0 & -\frac{1}{J} \\ 0 & 0 & 0 \end{bmatrix} \tag{4.24}$$

$$u = \begin{bmatrix} v_A & v_B & T_L \end{bmatrix}^t \tag{4.25}$$

4.2 Parameters of Electric Circuit and Mechanical System

Calculations of motor performance were carried out for the system parameters presented in Table 4.1

Table 4.1Parameters of electric circuit and mechanical system

$E_b = 300\ V$	emf of the battery
$R_s = 1.5\ \Omega$	source Resistance
$R_c = 2\ \Omega$	resistance in series with capacitor
$C = 10\,\mu F$	capacitance
$R_a = 8\ \Omega$	phase resistance of the brushless DC motor
$L_c = 0.021\text{H}$	phase resistance of the brushless DC motor
$K_e = 1.324$	emf constant
$J = 0.001\ Kg/m^2$	moment of inertia
$D = 0.001$ N/(rad/s)	friction coefficient
$T_{load} = 2.2 N.m$	load torque
$T_{mc} = 0.3\ N.m$	maximum cogging torque and $\beta = 0$
$T_s = 0.1\ N.m$	coulomb friction torque

4.3 Dynamic Simulation of the Motor

The simulation of the motor operation in dynamic conditions was done using software package MATLAB/SIMULINK®. The block diagram of the drive system which is shown in Figure 4.3 a, was developed using the mathematical model derived in section 4.1.

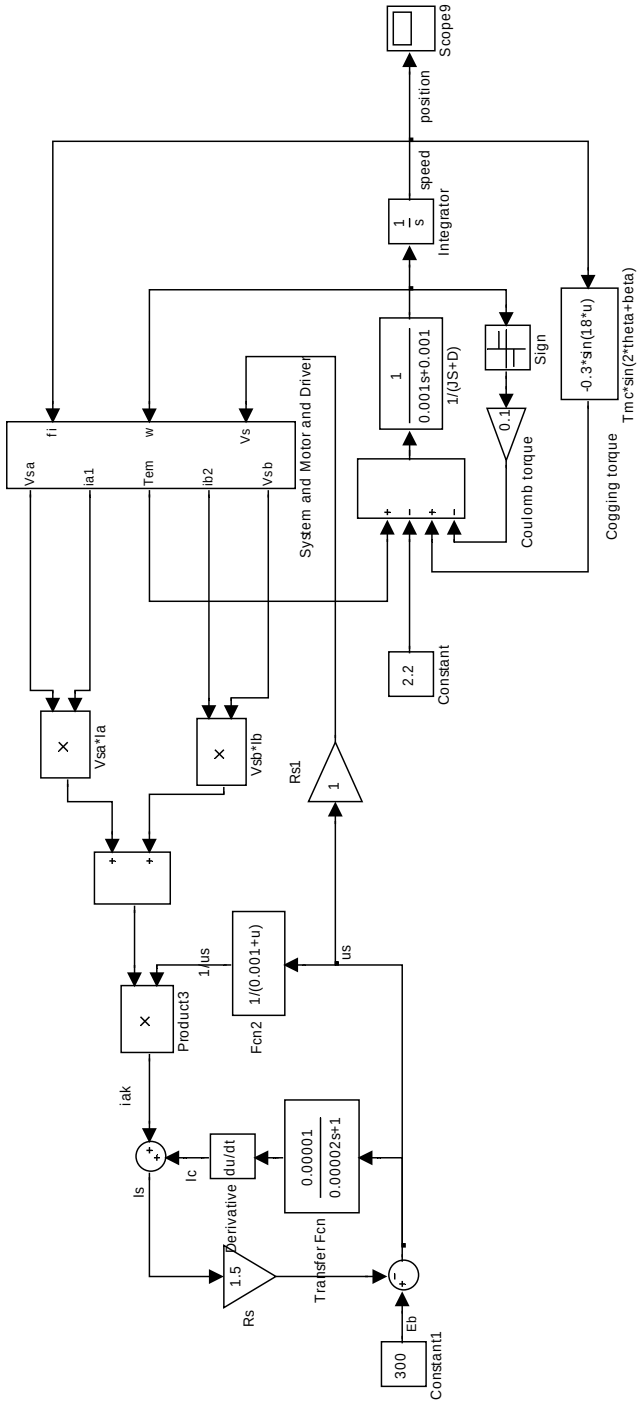

Figure 4.4 Simulink block of AFPM motor with two phase winding

The main block diagram consists of three parts: supply source, inverter + motor winding and mechanical system of the drive. The subsystem related to the inverter–motor circuit is shown in Figure 4.4

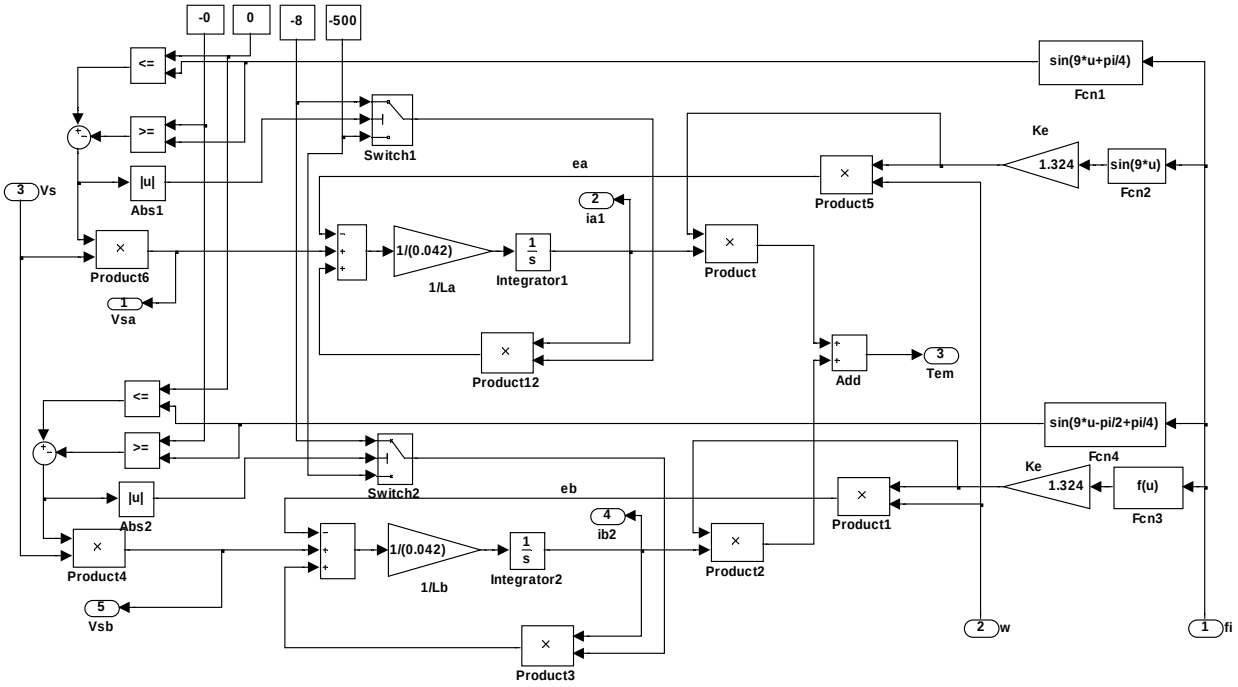

Figure 4.5 Simulink model of inverter-motor circuit subsystem.

4.3.1 Starting up Operation

To simulate this operation, it was assumed that: the drive system is supplied with constant voltage of 300 *V*, the system is loaded with the rated torque of 2.2 *N.m*, and the Switching angle is -30^0.

The simulation results of starting of the motor are shown in Figs 4.5, 4.6, 4.7, 4.8 and 4.9. In particular the Figure 4.5 shows the rotary speed (*n*) and source current (i_s) waveforms. The ripple in the speed waveform is due to the oscillation of motor torque. It consists of two components: electromagnetic torque T_{em} and cogging torque T_c. These

two components are shown in Figure 4.11, which were drawn when the motor reached steady state. The electromagnetic torque waveform obtained during the starting process is shown in Figure 4.10. The results presented in Figure 4.10 show that the torque developed by the motor is always positive despite the relatively big cogging components, as written in Chapter 2. This positive resultant torque is obtained due to displacement of PMs on one of the rotor discs.

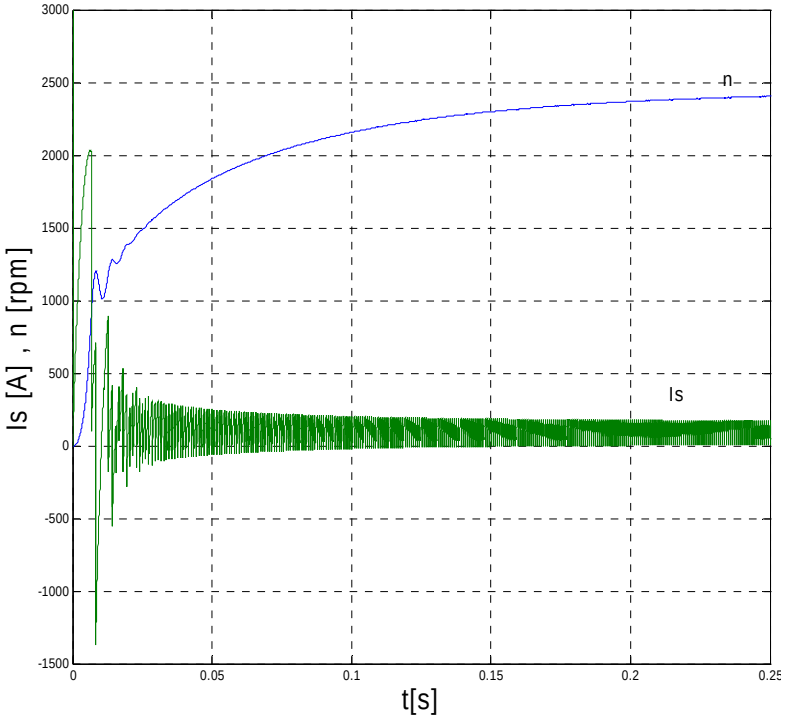

Figure 4.6 Waveform of rotary speed (n) and source current (i_s)

The waveform of EMF (e_a) and armature voltage (v_a) of phase A and the waveform of EMF (e_b) and the armature voltage (v_b) are shown in Figs 4.6 and 4.7. The induced EMF's and voltage applied to the motor are in phase because the winding was switched ON without any delay with respect to the position of magnets and winding.

Figure 4.8 and Figure 4.9 shows the current and voltage waveforms. The shape of current waveforms is far from being rectangular; it is influenced not only by supply voltage but also by the emf and by the winding inductance.

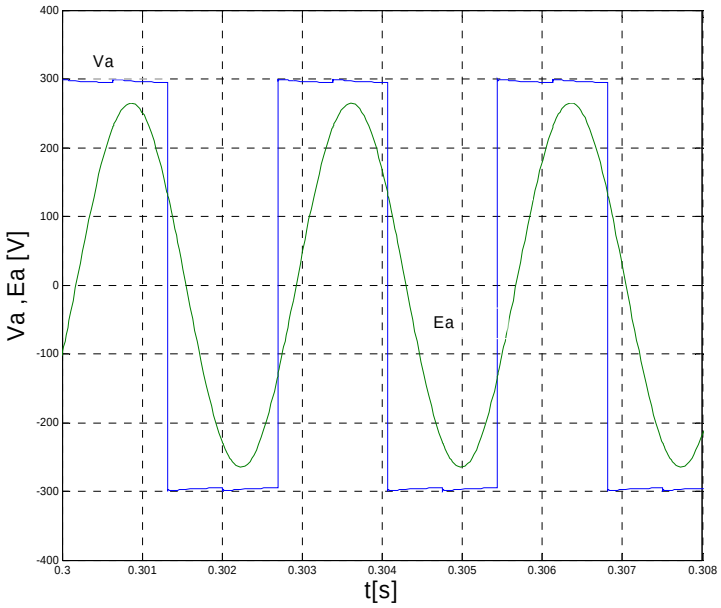

Figure 4.7 Waveform of EMF (e_a) and armature voltage (V_a)

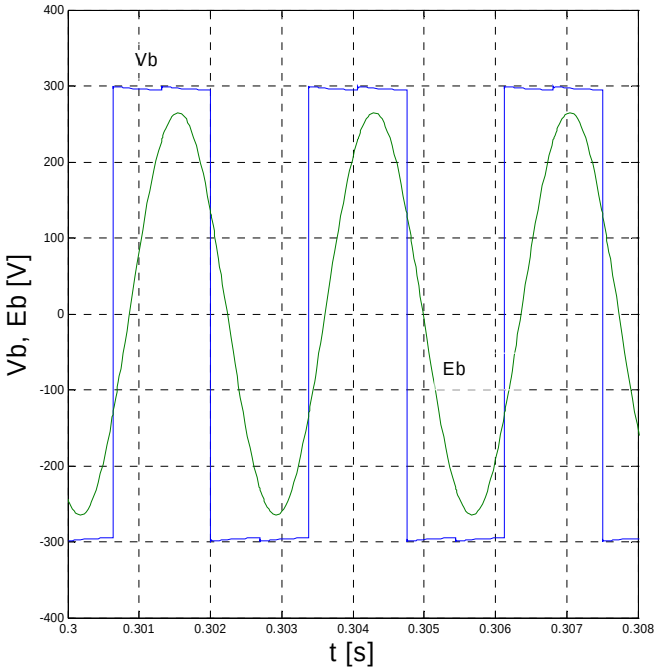

Figure 4.8 Waveform of EMF (e_b) and armature voltage (V_b)

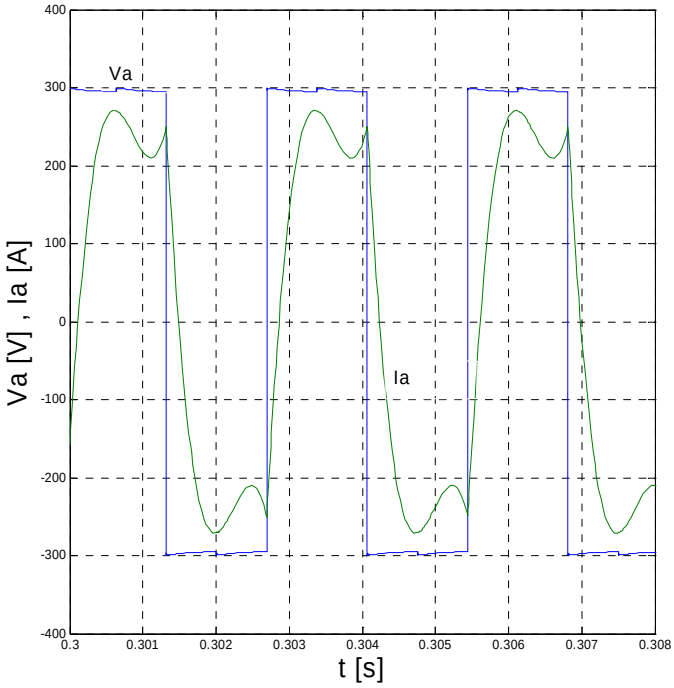

Figure 4.9 Waveform of armature current (i_a) and armature voltage (V_a)

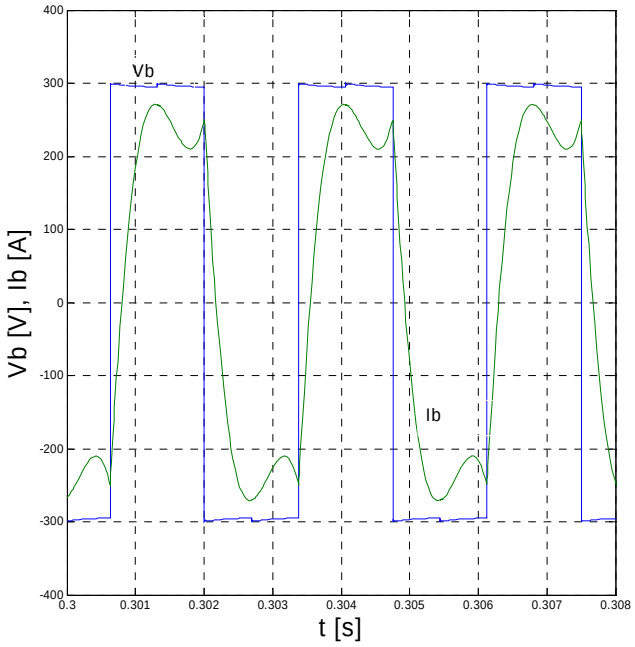

Figure 4.10 Waveform of armature current (i_b) and armature voltage (V_b)

The motor after starting process reaches the steady-state operation within 1 sec. The motor was loaded with the rated torque 2.2 *N.m*. Thus the values of other quantities

can be regarded as the rated ones. Their average values were calculated and listed in Table 4.2

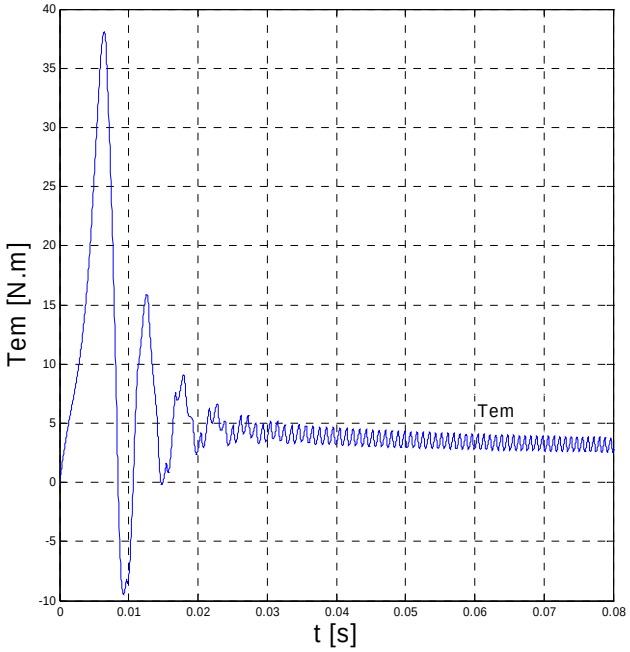

Figure 4.11 Waveform of electromagnetic torque (Tem)

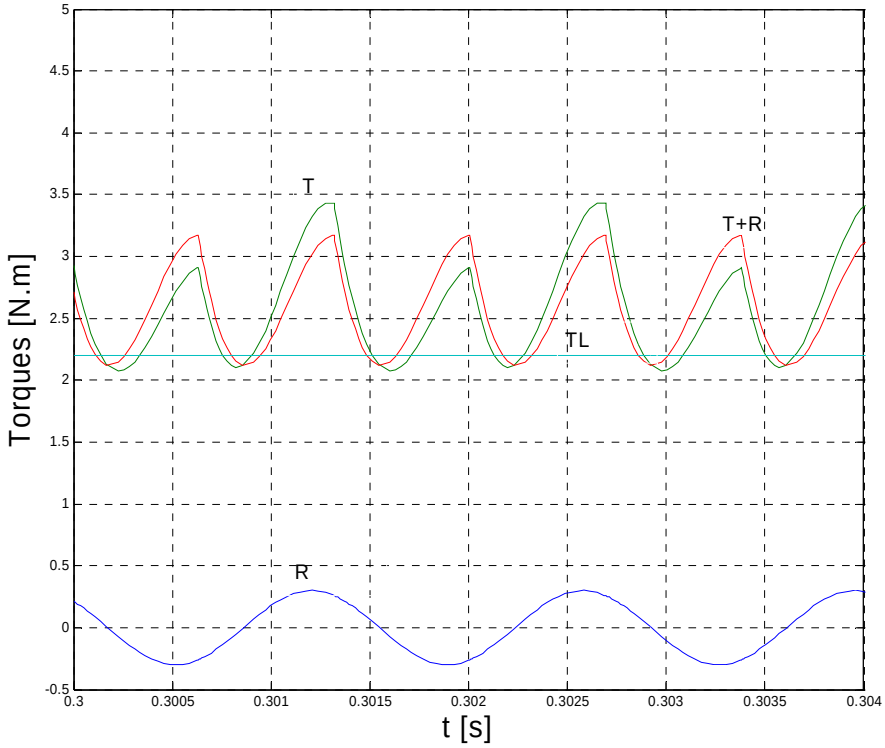

Figure 4.12 Waveforms of electromagnetic torque(T), cogging torque(R) and resultant torque(T+R)

The motor efficiency was calculated similar to the single-phase AFPM which was discussed in section 3.3.1. The electromechanical characteristics are calculated for different loads and switching angle (β=-30^0) which was shown in Figure. 4.12

Table 4.2Average values at rated torque 2.2 N.m

Supply Voltage	300 *V*
Output Power	563 *W*
Rotary speed	2445 *rpm*
Torque	
Efficency	2.2 *N.m*
	81.60 *%*

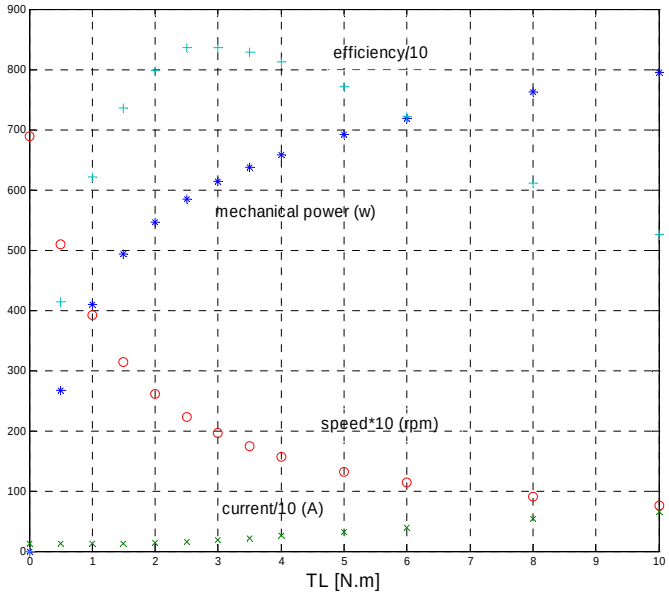

Figure 4.13 Electromechanical characteristics of motor at constant supply 300V and switching angle (β=-30^0)

CHAPTER 5 AFPM BLDC MOTOR PERFORMANCE IN STEADY STATE

5.1 Single –Phase AFPM Motor Model for Steady-State Operation

Referring to Figure. 3.10 the single-phase AFPM brushless dc motor has nonlinear speed-torque characteristic. Within the range of small values of torque it changes in the way to dc series motors. On the other hand, the armature current vs. torque characteristic is a straight line which is the feature of the PMDC motors. If the motor has the strong (high energy) permanent magnets mounted on the rotor surface, as it is for considered motor, the armature reaction flux does not influence much on the resultant flux in the air-gap. So the electromagnetic torque can be expressed by the formula:

$$T = K_T \cdot I_a - T_0 \tag{5.1}$$

Where,

T – electromagnetic torque,

K_T – constant,

I_a – average armature current,

T_0 – friction torque,

Normally when DC brushless motor is analyzed no inductance of the commutated winding is taken into account because at any instant only small part of this winding is commutated. In the BLDM with single-phase winding the current change its direction in the whole winding. This contributes to the additional voltage drop across the winding inductance. It means the winding inductance has to be taken in to the account also in

steady-state model of the motor which is shown in Figure.5.1. The voltage equation for this model is in the following form (5.2).

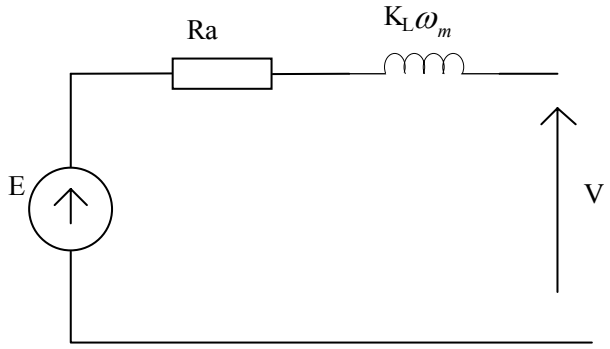

Figure 5.1 Equivalent circuit of the motor in the steady state conditions

The equations, which describe the motor model, are as follows:

$$V = E_a + I \cdot R_a + K_L \omega_m I_a^{\,n} \tag{5.2}$$

$$E_a = K_e \cdot \omega_m \tag{5.3}$$

From equations (5.2) and (5.3):

$$\omega_m = \frac{V - R.I}{K_E + K_L.I^n} \tag{5.4}$$

$$\text{Or} \quad \omega_m = \frac{V}{K_E} - R_a\left(\frac{T + T_0}{K_E.K_L}\right) \tag{5.5}$$

where,

E_a – line-to-line electromotive force,

ω_m – rotor angular speed,

K_e, K_L – constant,

R_a – armature resistance,

I_a – average armature current

V – source voltage.

n – Power of I_a

5.1.1 Performance Characteristics of the Motor

Referring to the motor model in section 5.1.1 the coefficients K_T, K_L, n have to be determined for the particular motor, on the basis of characteristics determined for the particular motor on the basis of characteristics determined from more realistic model as it is in this project. In order to find out constants K_T, T_0 the characteristic I_a –T in Figure. 5.2 is considered. From this characteristics K_T is calculated by the equation 5.4. T_0

$$K_T = \frac{\Delta I_a}{\Delta T} \tag{5.4}$$

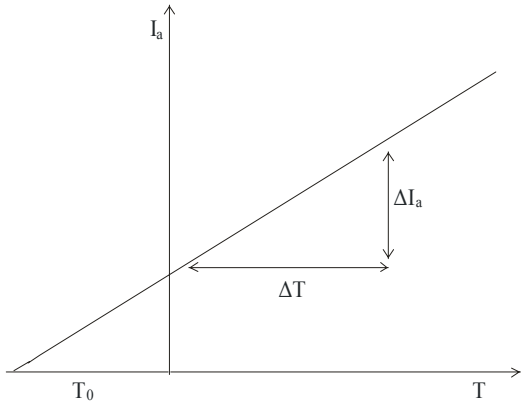

Figure 5.2 Torque versus current

The other parameters: n, K_L, (see table 5.1) were determined on the basis of try and error method where the steady-state characteristics obtained from equations 5.1-5.4. There are other methods for the estimation of the steady-state model parameters can be used which are faster but there are based on more complex procedure.

Using the equations in section 5.1, the program was written in MATLAB (see Appendix C file *single_steady.m*) to calculate the electromechanical characteristics. The

characteristics obtained from simulation at supply voltage 300 V and at switching angle $\beta = 0^{o}$ are shown in Figure. 5.2.

Table 5.1Steady-State Parameters

n	0.47
K_L	0.97
K_T	1.24
T_o	0.4

The mechanical power is calculated as follows

$$P_m = T_L \cdot \omega_m \tag{5.5}$$

The efficiency of the motor is

$$Eff_{\%} = \frac{P_{out}}{P_{in}} \cdot 100\% \tag{5.6}$$

where,

$$P_{out} = P_m - \Delta P_m \quad \text{- output power} \tag{5.7}$$

$$P_{in} = V \cdot I_a \quad \text{- input power} \tag{5.8}$$

In calculations, the mechanical power losses were expressed by the equation 5.8.

$$\Delta P_m = \omega_m{}^2 \cdot D \tag{5.9}$$

Where D is the friction coefficient of 0.001 (*Nm/(rad/s)*)

The current-torque characteristic is the straight line (Figure.5.3) which is due to the motor has the strong permanent magnets mounted on the rotor surface and has no armature reaction flux influence on the resultant flux in the air-gap. The speed-torque

characteristic is non-linear due to the presence of inductance in the armature. The electromechanical characteristics obtained from the measurements carried out on the motor prototype illustrate the performance similar to the dc shunt motor. With in the small range of torque it changes in to the way of dc series motors.

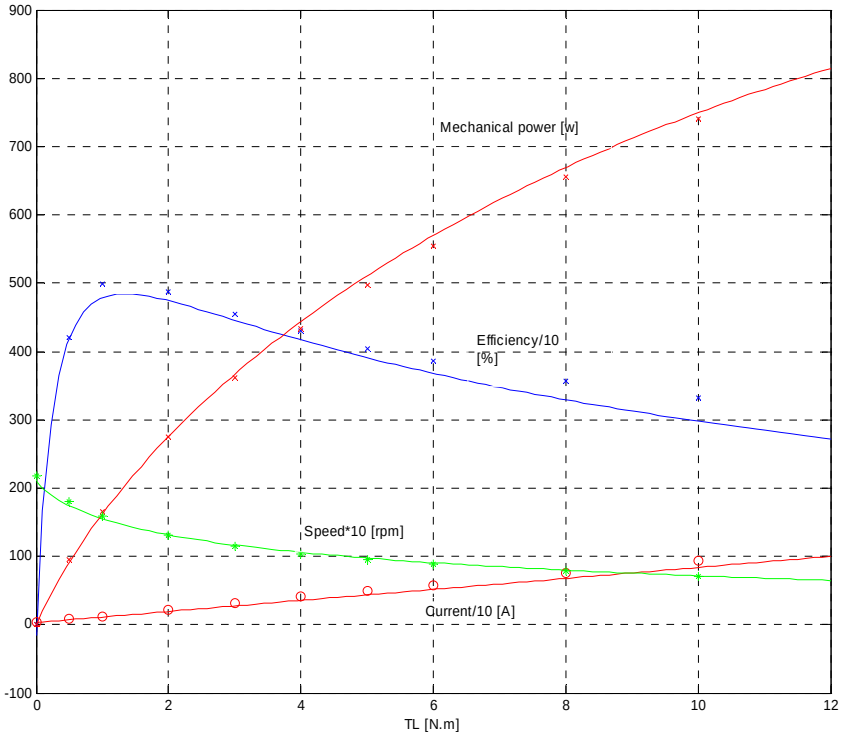

Figure 5.3 Electromechanical characteristics of Single-phase AFPM brushless dc motor supplied with 300 *V* voltage

5.1.2 An Influence of Switching Angle on Motor Performance

Due to the high-speed operation, the winding inductance causes a significant phase delay in the current waveform. The results in the current and the emf waveforms being out of phase, and a negative torque component is generated, with a consequent reduction of the overall torque. Due to the winding inductance the phase current cannot change instantaneously. There will be a period during which the emf and current have

opposite polarities and a negative component is produced. Figure.5.4 illustrates the relative phase of the emf and current waveforms when a conventional commutation strategy is employed. In order to get motor better performance Phase commutation advanced is often employed. In dc brush motor the commutation angle is determined by the position of brushes and is kept constant. In BLDC motors the switching angle may vary accordingly to the controller of the inverter that is used.

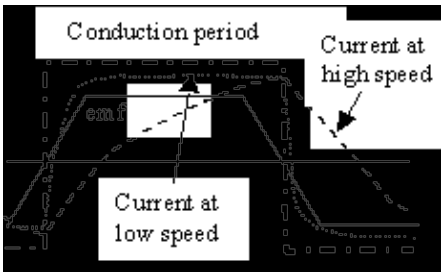

Figure 5.4 Current and emf waveforms

As the switching angle is advanced, the difference between back-emf and the supply voltage increases, and the torque thereby increases. However, there exists an optimal advanced angle, beyond which the drive performance deteriorates.

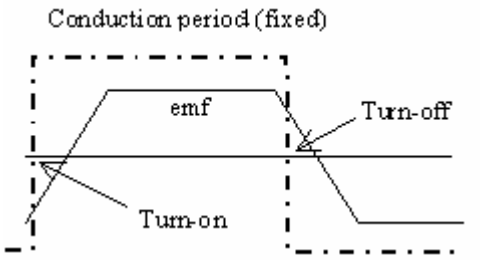

Figure 5.5 Phase advanced techinique

In the dynamic simulation it is easy to switch the inverter voltage v_{sa} than i_a . The switching angle β is referred to the emf waveform where e_a is equal to 0 (Figure. 5.6). The duty cycle is kept constant The influence of switching angle on the motor

performance the simulation was done for the following switching angles β = -$10^0, 20^0, 30^0, 40^0$.

The results of simulation were plotted in the form of characteristics of average values of the efficiency (*Eff*), input current (i_s) and mechanical power output (P_{em}) shown in Figs 5.7, 5.8 and 5.9.

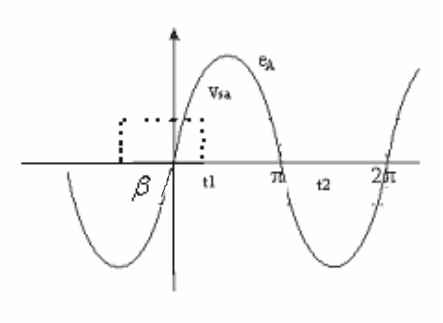

Figure 5.6 v_{sa} and e_a and β

The characteristics were drawn in the Matlab from the results obtained in simulation using dynamic model of the motor.

The efficiency was calculated as same as section 3.4.The motor efficiency is maximum when the switching angle β = -30^0 at load torque 4 *N.m*, which means transistors are switched much earlier and the motor efficiency is minimum when β = -10^0.

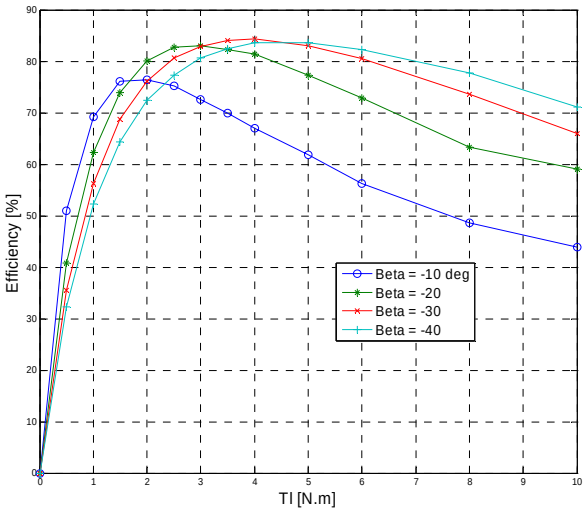

Figure 5.7 Efficiency (%) vs. load torque (TL)

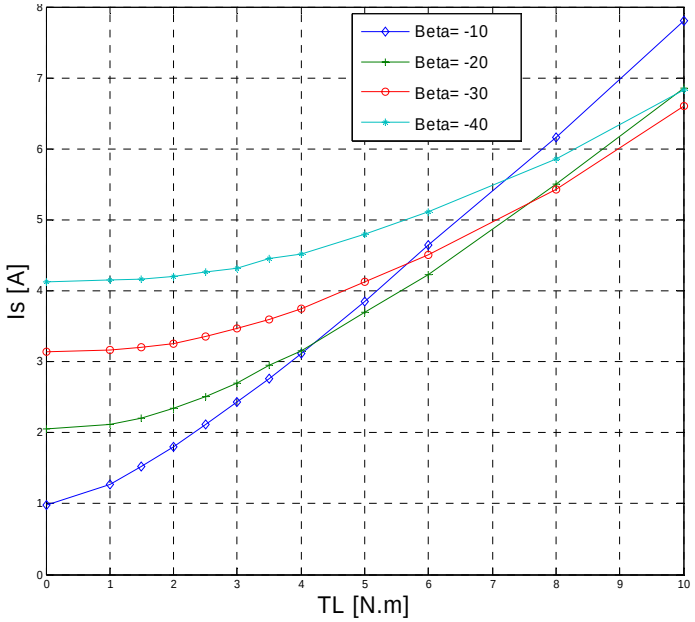

Figure 5.8 Input current (I_s) vs. Load torque (TL)

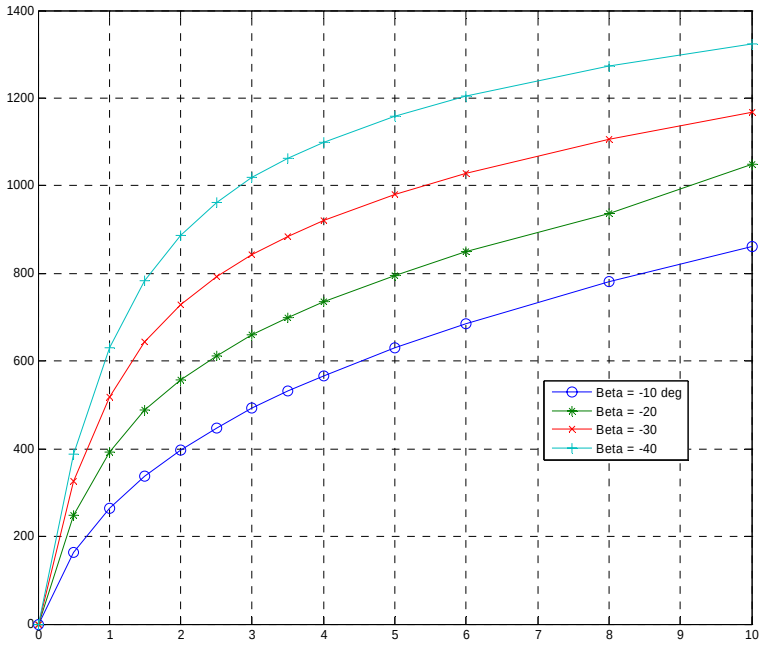

Figure 5.9 Mechanical power output (Pem) vs. load torque (TL)

Table 5.1 shows the Efficiency, Mechanical power and speed for different Switching angles (β) at rated torque 2.2 N.m.

Table 5.2 Speed, Efficiency and Mechanical power for different switching angles for T_L=2.2N.m

β (degrees)	Speed(rpm)	Eff(%)	Pem(W)
-10^0	1816	76.65	418
-20^0	2520	81.20	580
-30^0	3278	78.17	756
-40^0	3992	74.55	920

5.2 Two-phase AFPM Motor Model for Steady-State Operation

The electromechanical characteristics obtained from dynamic simulation which were shown in the section 4.2 are similar to the electromechanical characteristics of single-phase AFPM motor. Here speed-torque characteristics are non linear due to the inductance present in the armature. Due to the strong permanent magnets on the rotor there is no armature reaction and therefore the current and torques is a straight line.

The equations, which describe the motor model, are similar which are discussed in section 5.1.

5.2.1 Performance Characteristics

The calculations to calculate K_T, K_L, n (see table 5.2) are similar to the calculations which was discussed in section 5.1.1. The program was written in MATLAB (see Appendix C file *two_steady.m*) to calculate the electromechanical characteristics. The characteristics obtained from simulation at supply voltage 300 V and at switching angle $\beta = 0^o$ are shown in Figure. 5.10. The maximum speed at no-load is less when compared to speed in single-phase motor.

Table 5.3 Steady state parameters for two-phase motor

n	0.47
K_L	0.97
K_T	1.24
T_o	0.4

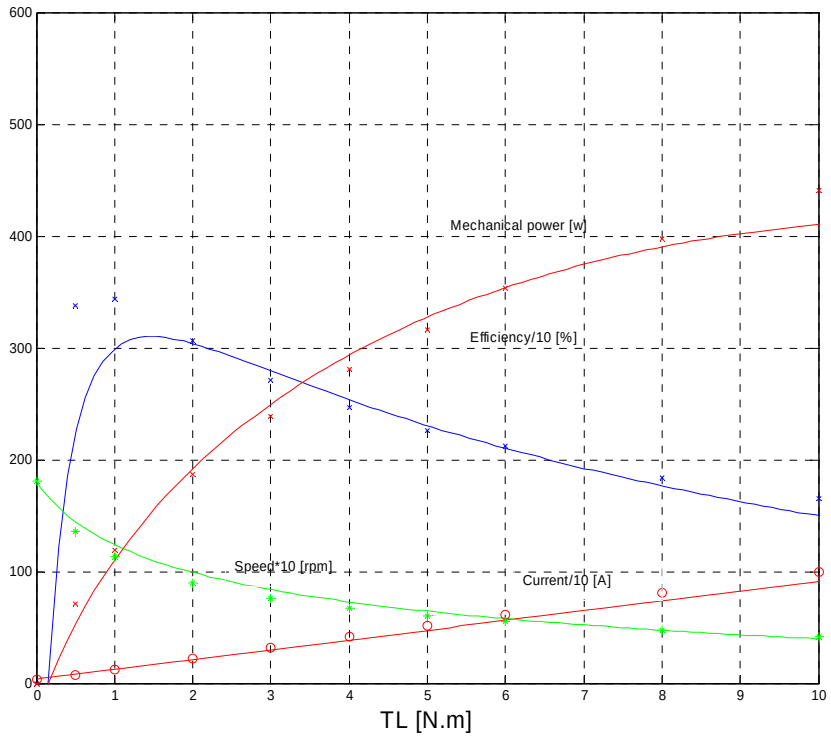

Figure 5.10 Electromechanical characteristics of two-phase AFPM brushless dc motor supplied with 300 *V* voltage

5.2.2 An Influence of Switching Angle on Motor Performance

The winding inductance causes significant phase delay on current waveform in both the phases i_a, i_b. The results in the currents and the emfs waveforms being out of phase, and a negative torque component is generated, with a consequent reduction of the overall torque. In order to get motor better performance both the phases are switched earlier.

The simulation was done for the following switching angles $\beta = 20^0, 30^0, 40^0$ and 45^0 which means transistors are switched are switched earlier. The results of simulation were plotted in the form of characteristics of average values of the efficiency (*Eff*), input current (Is), speed (n) and mechanical power output (P_{em}) in Figs. 5.11, 5.12, 5.13 and 5.14. The efficiency was calculated in the same way as in single- phase (see equation

3.19). The motor efficiency is higher when the switching angle $\beta = -40^0$ at load torque 4 *N.m,* which means transistors are switched much earlier.

The motor efficiency has minimum when $\beta = -20^0$. Table 5.2 shows the efficiency, mechanical power and speed for different switching angles (β) at rated torque 2.2 N.m

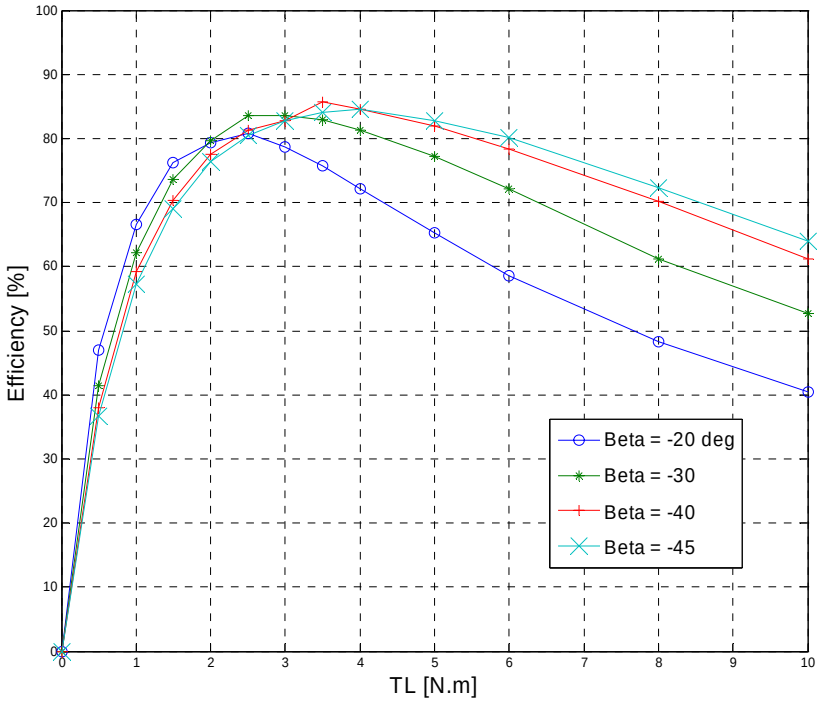

Figure 5.11 Efficiency(E_{ff}) vs load torque(TL)

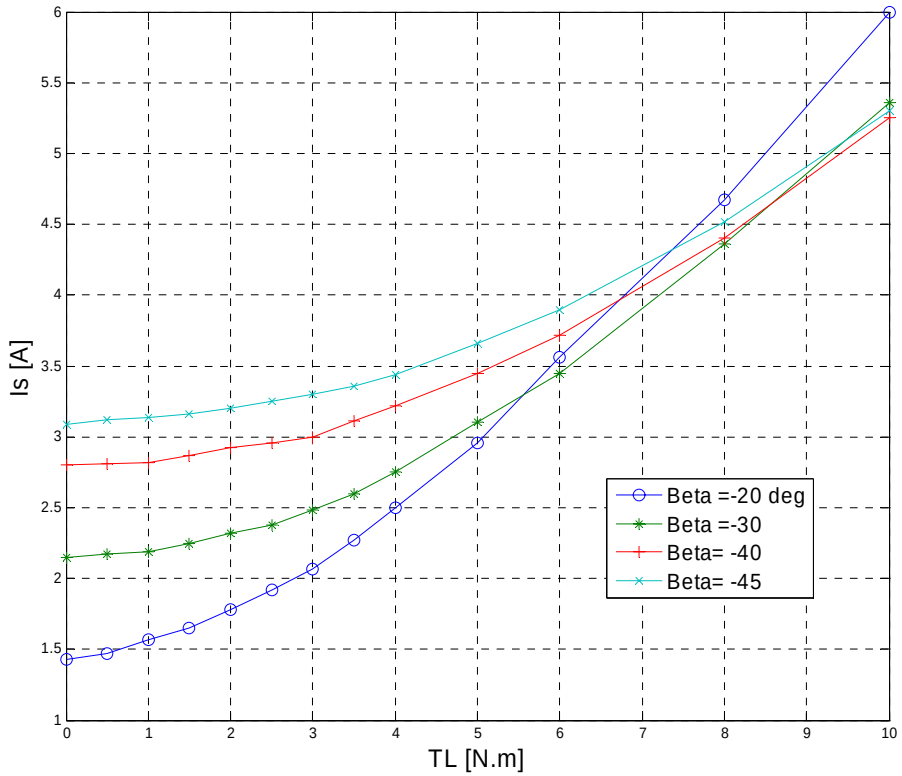

Figure 5.12 Input current(I_s) vs load torque(TL)

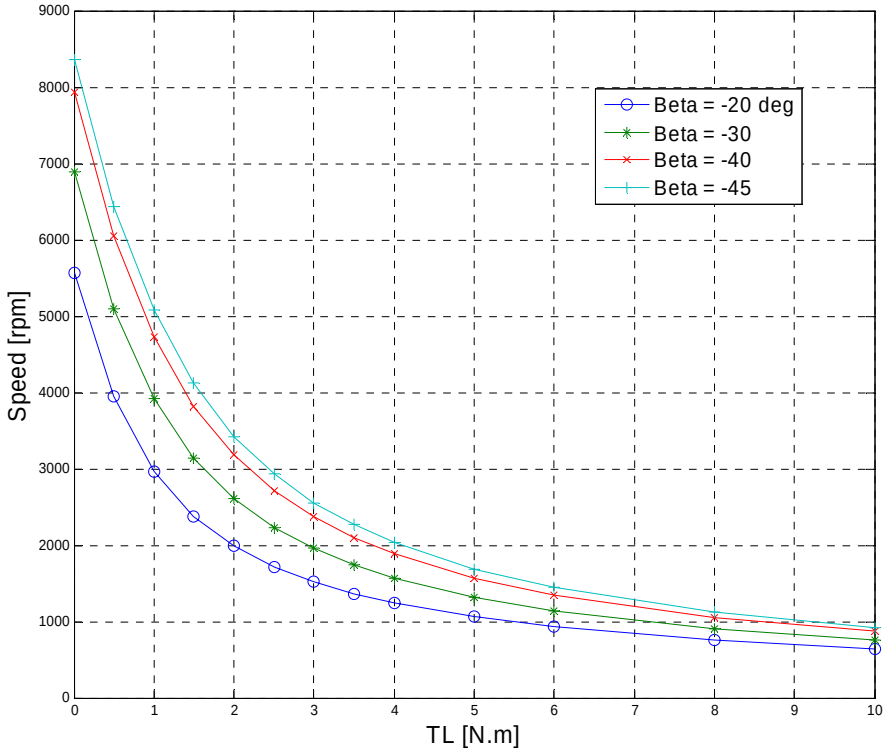

Figure 5.13Speed (rpm) vs load torque (TL)

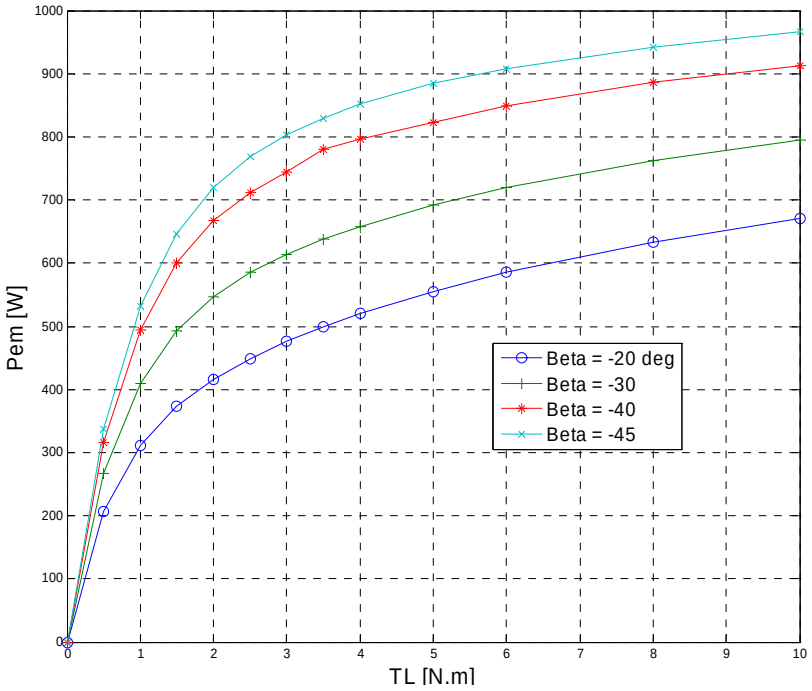

Figure 5.14 Mechanical power output (Pem) vs. load torque (TL)

Table 5.4Speed, efficiency and mechanical power for different switching angles at rated T=2.2 N.m

β (degrees)	Speed(rpm)	Eff(%)	Pem(W)
-20^0	1868	80.82	430
-30^0	2447	81.59	563
-40^0	2980	79.67	686
-45^0	3218	78.74	741

5.3 Comparison of the AFPM Motor Performance at Single-phase and Two-phase Connection

The AFPM BLDC motor considered in this project was analyzed in two versions, as a single-phase and two-phase motor. Their stator and motor structures are the same. They differ only in winding connection, and the type of converter. However, their performance differs too. Comparing the results obtained from simulation in dynamic condition and steady-state condition the following conclusions can be deducted.

- The electromechanical characteristics of the AFPM brushless DC motor with single-phase and two-phase winding look similar, the speed-torque characteristics are non linear in both the cases and this is due to the influence of the stator winding inductance. The current-torque characteristics are almost a straight line in both the cases which is due to as there is no armature reaction.
- In the single phase configuration the torque which was shown in the Figure. 3.9. has more ripples compare to the torque developed in the two-phase case which was shown in the Figure. 4.9. So AFPM motor at single-phase configuration is not applicable in such drives where smooth torque is required. AFPM motor with single-phase winding can be used for the pumps where the ripples in the torque are not much importance. AFPM motor with two-phase winding may be used in the drives where smoother torque is required.
- At rated torque 2.2 *N.m* The rotor in the AFPM brushless dc motor with single-phase winding reaches steady speed (Figure. 3.5) in a relatively shorter time compared to the AFPM motor with two-phase winding. (Figure. 4.5)

- The Efficiency at rated torque 2.2 *N.m* is higher for the AFPM motor with two-phase winding than AFPM motor with single-phase winding but the mechanical power and the speed developed is higher in single-phase than in two-phase case.
- At rated torque 2.2 *N.m,* the speed reached at steady state is higher in single-phase AFPM BLDC motor than the speed reached at steady state in two-phase AFPM BLDC.
- The motor performance in both the cases can be improved by changing the switching angle (β) (see section 5.1.2). It is observed that by advancing the phase commutation the motor performance improved tremendously in both single-phase AFPM motor and two-phase AFPM motor. It is observed that in single-phase motor the higher efficiency (84.40 %) is achieved at switching angle (β) = -30^0 at load torque 4 *N.m*. In the two-phase motor the higher efficiency (85.71 %) is achieved at switching angle (β) = -40^0 at load torque 3.5 *N.m*.
- The problem of starting torque in the single-phase motor is eliminated by rearranging the position of magnets on one of the rotor disc which was discussed in chapter 2. In case of two-phase motor the staring torque is not at all problem and there is no need rearrange rotor magnets on one of the rotor disc.
- The advantage of single-phase machine is the simpler commutator where as in the case of two-phase the commutator is some what complex.

CHAPTER 6 CONCLUSIONS

The performances of the AFPM BLDC motor with single-phase and two-phase winding were analyzed in this thesis. To study the motor operation, a mathematical dynamic model has been proposed for both the cases. This model became the basis for block diagram and simulations, which were performed using MATLAB/SIMULINK software package.

The results obtained from the simulation in steady-state allowed to draw the electromechanical characteristics, which illustrates the motor performance. These characteristics were the basis for determination of the simpler motor model, which is normally used to analyze the conventional brush DC machines.

The results obtained from dynamic model and steady-state model enabled to compare both types of motors and deduct the following conclusions.

- In single-phase motor the cogging torque is very high and it contributes to an increase of the torque ripple. It makes the motor inapplicable where smooth torque is required. However it can be used in the drives which do not demand smooth torque like pumps, fans, etc.
- The two-phase motor develops the torque with lower ripple but still it cannot be applied where this cannot be tolerated e.g. wheelchair
- The advantage of the single-phase motor is the simpler commutator, which needs only one position sensor and four transistors; where as in two-phase motor two sensors and 8 transistors are necessary which makes the circuit more complex.
- The results of simulation at rated torque show the AFPM motor with two-phase winding has higher efficiency than the AFPM motor with single-phase winding.

- A study done on the influence of switching angle on motor performance shows that motors operate better when the windings are switched ON earlier with respect to the emfs induced in them. It means the inverters should operate at the advanced switching angle if voltage inverters are applied and preferably for the motor analyzed in this project at angle β=*-30*

Future work is to include Mems technology in the electronic commutator so that complexity of the circuit is minimized and rearrange the geometric of the magnets so the resultant torque will have fewer ripples.

REFERENCES

[1] T. Kenjo and S. Nagamori, *Permanent – magnet and Brushless DC Motors*, Clarendon Press, Oxford, 1985.

[2]BrushlesDCmotors– **http://services.eng.uts.edu.au/~joe/subjects/ems/ems_ch12_nt.pdf**.

[3] Jacek F. Gieras, Rong-Jie Wang, Maarten J. Kamper, *Axial flux permanent magnet brushless machines,kluwer academic publications,2004.*

[4] A. Parviainen, M. Niemelä, J. Pyrhönen. "Modeling Axial-flux Permanent-Magnet Machines". *IEEE Transaction on Industry Applications*. Vol. 40, No. 5, 2004, pp. 1333-1340.

[5] A. Parviainen, M. Niemelä, J. Pyrhönen. "Design of Axial-flux Permanent Magnet Machines: Thermal Analysis". In *Proceedings of International Conference on Electrical Machines*, ICEM'04, Cracow, Poland, 5-8 September 2004, on CD-ROM.

[6] R. Drzewoski and E. Mendrela, "Torus type brushless D.C. motor as a gearless drive for electric vehicles.

[7] R. Drzewoski, J. Jelonkiewicz and E.A. Mendrela, "Gearless drive for electric vehicles with disc motor", *Electrical Engineering News* 1999 ,no. 4, pp. 188 - 193.

[8] E. Mendrela, J. Moch, P. Paduch, "Performance of disc-type brushless DC motor with single-phase winding", *Archives of Electrical Engineering,* vol. L, no. 2, pp. 145-153, 2001.

[9] E. Mendrela, M. Łukaniszyn and K. Macek-Kamińska, *Disc-Type Brushless DC Motors*, Polish Academy of Science, 2002.

[10] E. Mendrela and R. Drzewoski, "Performance of stator salient pole disc brushless DC motor for EV", *Power Electronics and Variable Speed Drives,* Conference Publication no. 475 IEE 2000, 18-19 September 2000.

[11]E. Mendrela, R. Beniak and R. Wrobel, "Influence of Stator Structure on Electromechanical Parameters of Torus-Type Brushless DC Motor",*PE-386EC*, 1999.

[12] E. Mendrela ,M.Jagiela "Analysis of torque developed in Axial flux, Single-Phase Brushless DC motor with Salient-pole Stator". IEEE Transsactions on energy conversation,Vol. 19,NO.2,JUNE 2004.

[13] E. Mendrela and R. Drzewoski, "Performance of stator salient pole disc brushless DC motor for EV", *Power Electronics and Variable Speed Drives,* Conference Publication no. 475 IEE 2000, 18-19 September 2000.

[14] R. Krishnan, *Electric Motor Drives Modelling, Analysis and Control*, Printice Hall, Inc., 2000

[15].J.F.Gieras and M. Wing*, Permanent magnet motor technology – Design and Applications Second Edition, Revised and Expanded*, Marcel Dekker, Inc., New York, Basel.

APPENDIX A: MATLAB PROGRAMS FOR SINGLE-PHASE MOTOR

Program 1:

```
%Electromechanical characteristics of the motor (Dynamic State)
% TL - T_load
% pin - Input power
% Pem - Mechanical Power
% is - Source Current
% ia - Armature Current
% w - Speed
% eff - efficiency
% Tem - Electromagnetic Torque

% Switching angle Beta=-20
TL=[0 0.5 1 1.5 2 2.5 3 3.5  4 5 6 8 10];
pin2=[600 607 630 660 696 740 793.5 850 904 1030 1168 1480 1780];
pem2=[0 248 392.52 487.5 557.34 612.5 659.3 699.8 735.6 795.5 850.4 937.4 1050];
is2=[ 2.05 2.06 2.12 2.21 2.35 2.51 2.7 2.95 3.15 3.7 4.23 5.5 6.86];
ia2=[ 4.6 2.99 2.68 2.76 3.23 3.87 4.66 5.38 6.9 8.4 11.2 13.71 ];
n2=[6345 4949  4210 3400 3004  2681  2340.8 2110  1910  1610 1415 1120 980 ];
eff2=[0 40.85 62.30 73.86 80.07 82.77 83.08 82.32 81.37 77.23 72.80 63.33 58.98];

% Switching angle Beta=-30
Tl=[0 0.5  1 1.5 2 2.5 3 3.5 4  5 6 8 10];
pin3=[910 915 922 936 956 981 1016 1052 1090  1180 1278 1505 1770];
pem3=[0 325.5  518 643 728 792 842.1 884 920  980 1029.1 1107 1167];
is3=[3.14 3.15  3.16 3.2 3.26 3.36 3.47 3.6 3.75 4.13 4.5 5.43 6.6];
ia3=[3.2 3.35 3.5 3.62 3.72 3.815 4.01 4.34 4.76 5.85 7.05 9.56 12.00 ];
n3=[8036 6220 4946 4087 3475 3027 2680 2412 2196 1871 1631 1322 1114 ];
eff3=[0 35.57 56.18 68.69 76.15 80.73 82.88 84.03 84.40 83.05 80.52 73.55 65.93  ];

% Switching angle Beta=-10
Tl=[0 0.5 1 1.5 2 2.5 3 3.5 4 5 6 8 10 ];
pin1=[285 320 377 450 520 610 678 760 846 1021 1220 1575 1960];
pem1=[0 163 264.5 338 397.6 447 492 531 567 630.9 686 781.5 861];
is1=[0.98 1.1 1.276 1.52 1.8 2.12 2.43 2.76 3.12 3.85 4.65 6.16 7.8];
ia1=[2.7 1.8 2.73 3.85 4.9 5.95 6.9 7.83 9.51 11.05 13.84 16.2 ];
n1=[4216 3124 2527 2153 1899 1710 1566 1450 1354 1205 1092 933 822 ];
eff1=[0 50.93 69.15 76.11 76.46 75.15 72.55 69.86 67.04 61.79 56.22 48.6 43.92];

% Switching angle Beta=-40
Tl=[0 0.5 1 1.5 2 2.5 3 3.5 4  5 6 8 10];
pin4=[1200 1202 1204 1215 1226 1245 1262 1288 1316 1385 1462 1636 1862];
pem4=[0 388 630 782.7 887.36 962 1018 1062.5 1100 1158.3 1204 1272.8 1323];
is4=[4.13 4.14 4.15 4.17 4.2 4.26 4.32 4.46 4.52 4.8 5.11 5.86 6.83];
```

```
ia4=[5.93 5.3 5.0 4.86 4.82 4.86 5.03 5.25 5.98 6.88 8.97 11.16 ];
n4=[9356 7420 6021 4982 4238 3675 3241.7 2900 2626.43 2212.7 1916.5 1520 1263];
eff4=[0 32.33 52.32 64.41 72.37 77.26 80.66 82.49 83.58 83.63 82.35 77.79 71.05];

figure(1)
plot(TL,eff1,'-r*',TL,eff2,'-b^',TL,eff3,'-ko',TL,eff4,'-go',), grid
xlabel('TL[N.m]');
ylabel('%Efficiency');
legend('Beta=-10','Beta=-20','Beta=-30','Beta=-40',4)

figure(2)
plot(TL,is1,'-r*',TL,is2,'-b^',TL,is3,'-ko',TL,is4,'-go'), grid
xlabel('TL[N.m]');
ylabel('supply current');
legend('Beta=-10','Beta=-20','Beta=-30','Beta=-40', 4)

figure(3)
plot(TL,pem1,'-r*',TL,pem2,'-b^',TL,pem3,'-ko',TL,pem4,'-go'), grid
xlabel('TL[N.m]');
ylabel('mechanical power output');
legend('Beta=-10','Beta=-20','Beta=-30','Beta=-40',4)


figure(4)
plot(TL,n1,'-r*',TL,n2,'-b^',TL,n3,'-ko',TL,n4,'-go'), grid
xlabel('TL[N.m]');
ylabel('mechanical power output');
legend('Beta=-10','Beta=-20','Beta=-30','Beta=-40',4)
```

Program 2:

```
% simulation results-steady state model
Tl=[0 0.5 1 2 3 4 5 6 8 10];
pin=[98 226 333 565 794 1010 1230 1440 1835 2225];
pem=[0 95 166.14 275.64 361 434 498 555 655 740];
is=[0.35 0.85 1.26 2.2 3.15 4.1 5.0 5.8 7.6 9.3];
ia=[2.3 4.1 5.54 8.00 10.05 11.7 13.3 14.7 17.1 19.2];
n=[2184 1810 1586 1316 1151 1036 951 884 782 708];
eff=[0 42.03 49.96 48.78 45.46 42.97 40.48 38.54 35.69 33.25];


KL=0.95;
Is=0.2:5/50:10; Kms=1.24;
%Us=270;Rs=4;
Us=300;Rs=5.5;%Ra+Rs=4+1.5;
Ps=Us*Is;
omgas=(Us-Rs*Is)./(0.65*Kms+KL*Is.^0.47);
```

```
ns=omgas*30/pi;
Ts=Is.*Kms-0.4;
Pms=(Is.*Kms-0.4).*omgas;%omgas*.002)%0.0025
Effs=Pms./Ps*100;
figure(1),
plot(Ts,Effs*10,'b',Ts,10*Is,'r',Ts,ns/10,'g',Ts,Pms/1,'r',Tl,eff*10,'xb',Tl,10*is,'ro',Tl,pem,'
rx',Tl,n/10,'g*'),grid,
xlabel('torque  [Nm]'),gtext('efficiency  [%]'),gtext('speed  [r.p.m.]'),
gtext('mechanical power  [W]'),gtext('current/10 [A]')
```

APPENDIX B: MATLAB PROGRAMS FOR TWO-PHASE MOTOR

Program 1:

```
%Electromechanical characteristics of the motor (Dynamic State)
% TL - T_load
% pin - Input power
% Pem - Mechanical Power
% is - Source Current
% ia - Armature Current
% n - Speed
% eff - efficiency
% Tem - Electromagnetic Torque


%  Switching angle Beta=-30
Tl=[0 0.5 1 1.5 2 2.5 3 3.5 4 5 6 8 10];
pin2=[642 645 660 670 686 700 735 770 810 897 996 1238 1510];
pout2=[0 267.22 410 493 547 585 614 638 658 692 719 762 795];
is2=[2.15 2.17 2.19 2.25 2.32 2.38 2.48 2.6 2.75 3.1 3.45 4.36 5.36 ];
ia2=[1.27 1.28 1.29 1.31 1.36 1.56 1.84 2.18 2.52 3.23 3.93 5.34 6.6 ];
n2=[6896 5100 3922 3142 2612 2235 1956 1742 1572 1321 1144 910 758 ];
eff2=[0 41.42 62.12 73.58 79.73 83.57 83.60 82.85 81.23 77.14 72.18 61.15 52.64];

% Switching angle Beta=-40

Tl=[0 0.5 1 1.5 2 2.5 3 3.5 4 5 6 8 10];
pin3=[840 834 836 853 861 875 900 910 942 1005 1082 1262 1492];
pout3=[0 316.5 495 600 667 712 745 780 796 823.4 848.4 885.8 912.0];
is3=[2.80 2.81 2.82 2.87 2.92 2.96 3.0 3.11 3.22 3.45 3.72 4.4 5.25 ];
ia3=[ 1.6 1.6 1.63 1.67 1.74 1.88 2.09 2.34 2.9 3.48 4.69 5.9];
eff3=[7929 6045 4729 3823 3182 2718 2370 2101 1888 1572 1350 1057 871 ];
n3=[0 37.94 59.25 70.33 77.46 81.37 82.77 85.71 84.50 82.00 78.41 70.19 61.12];

% Switching angle Beta=-20
Tl=[0 0.5 1 1.5 2 2.5 3 3.5 4 5 6 8 10];
pin1=[431 438 467 489 525 556 605 660 721 850 998 1310 1660];
pout1=[0 206 311 373 416.4 449.34 476 499.5 520 555 585 632.5 670];
is1=[1.43 1.47 1.57 1.65 1.78 1.92 2.07 2.27 2.5 2.96 3.56 4.67 6.0 ];
ia1=[1.42 0.92 1.06 1.46 1.93 2.34 2.8 3.26 4.12 4.94 6.43 7.8];
n1=[5572 3942 2970 2378 1988 1716 1516 1362 1241 1060 930 754 640 ];
eff11=[0 47.03 66.59 76.27 79.31 80.81 78.67 75.68 72.12 65.29 58.61 48.28 40.36];

% Switchine angle Beta=-45

Tl=[0 0.5 1 1.5 2 2.5 3 3.5 4 5 6 8 10];
```

```
pin4=[ 918 920 928 937 941 954 970 988 1008 1067 1132 1302 1508];
pout4=[0 337 532 647 720 768 803.5 830 852 884 908 942.3 966];
is4=[3.09 3.12 3.14 3.16 3.2 3.25 3.3 3.36 3.44 3.66 3.9 4.52 5.3];
ia4=[1.96 1.82 1.80 1.81 1.89 1.97 2.16 2.36 2.85 3.4 4.51 5.68];
n4=[ 8355 6438 5077 4120 3426 2935 2557 2265 2032 1687 1444 1125 923 ];
eff44=[0 36.63 57.32 69.05 76.40 80.50 82.83 84.00 84.52 82.84 80.21 72.37 64.05];
figure(1)

figure(1)
plot(TL,eff1,'-r*',TL,eff2,'-b^',TL,eff3,'-ko',TL,eff4,'-go',), grid
xlabel('TL[N.m]');
ylabel('%Efficiency');
legend('Beta=-20','Beta=-30','Beta=-40','Beta=-45',4)

figure(2)
plot(TL,is1,'-r*',TL,is2,'-b^',TL,is3,'-ko',TL,is4,'-go'), grid
xlabel('TL[N.m]');
ylabel('supply current');
legend('Beta=-20','Beta=-30','Beta=-40','Beta=-4


figure(3)
plot(TL,pem1,'-r*',TL,pem2,'-b^',TL,pem3,'-ko',TL,pem4,'-go'), grid
xlabel('TL[N.m]');
ylabel('mechanical power output');
legend('Beta=-20','Beta=-30','Beta=-40','Beta=-45',4)


figure(4)
plot(TL,n1,'-r*',TL,n2,'-b^',TL,n3,'-ko',TL,n4,'-go'), grid
xlabel('TL[N.m]');
ylabel('mechanical power output');
legend('Beta=-20','Beta=-30','Beta=-40','Beta=-45',4)
```

Program 2:

```
% simulation results-steady state model
Tl=[0 0.5 1 2 3 4 5 6 8 10]
Pin=[94.5 210 346 610 880 1140 1400 1660 2170 2670];
pem=[0 71 119 187 239 281 316 353 398 441];
is=[0.34 0.75 1.25 2.2 3.2 4.15 5.12 6.1 8.1 10.0];
ia=[1.36 2.56 3.54 5.0 6.23 7.25 8.2 9.0 10.5 11.8];
n=[1810 1361 1136 896 761 670 604 553 476 421];
eff=[0 33.80 34.39 30.65 27.15 24.64 22.57 21.26 18.34 16.51];
KL=1.1;
Is=0.2:5/50:10; Kms=1.14;
%Us=270;Rs=4;
```

```
Us=300;Rs=9.5;%Ra+Rs=4+1.5;
Ps=Us*Is;
omgas=(Us-Rs*Is)./(0.86*Kms+KL*Is.^0.60);
ns=omgas*30/pi;
Ts=Is.*Kms-0.4;
Pms=(Is.*Kms-0.55).*omgas;%omgas*.002)%0.0025
Effs=Pms./Ps*100;
figure(1),
plot(Ts,Effs*10,'b',Ts,10*Is,'r',Ts,ns/10,'g',Ts,Pms/1,'r',Tl,eff*10,'xb',Tl,10*is,'ro',Tl,pem,'
rx',Tl,n/10,'g*'),grid,
xlabel('torque  [Nm]'),gtext('efficiency  [%]'),gtext('speed  [r.p.m.]'),
gtext('mechanical power  [W]'),gtext('current/10 [A]')
```

VITA

Sunil Kumar Challa was born in Guraja, India. He graduated from Vignan Institute of Technology and Science, an affiliate to Jawaharlal Nehru Technological University in Hyderabad, India, with a degree of Bachelor of Technology in Electrical and Electronics Engineering in 2003. In January 2004 he came to Louisiana State University to pursue graduate studies in electrical engineering. He will be awarded the degree of Master of Science in Electrical Engineering in August 2006.